Candida albicans epithelial invasion induces host membrane rupture at distinct subcellular niches following priming by the fungal toxin candidalysin

Noa Conan[1], Laura Marthe[1], Anouck Shekoory[1], Patricia Latour-Lambert[2], Jean-François Franetich[1], Martin Larsen[1], Allon Weiner[1]

[1]Sorbonne Université, CNRS, Inserm, Centre d'immunologie et des maladies infectieuses, CIMI, 75013 Paris, France

[2]Institut Pasteur, Unité Dynamique des interactions hôtes-pathogènes and Centre National de la Recherche Scientifique (CNRS) UMR3691, Université de Paris Cité, Paris, France

Abstract

Candida albicans is an opportunistic fungal pathogen normally found as a commensal in human mucosa. In susceptible patients, its hyphal filamentous form can invade and damage host epithelium leading to local or systemic infection. The secreted fungal toxin candidalysin is required for epithelial damage, although both hyphal extension and candidalysin are required for inducing maximal infection damage, for reasons that are not well understood. Here we study the interplay between hyphal extension and host damage *in vitro* using live cell imaging combined with damage-sensitive reporters followed by single-cell level quantitative analysis. We show that fungal load is inversely proportional to single-cell damage potential, and we quantify candidalysin-induced damage. We then determine the three-dimensional architecture of invasion and show that the spatial organization of host membrane rupture is regulated by candidalysin and is predictive of host cell death. Finally, we demonstrate that membrane rupture occurs at two distinct host subcellular niches: the juxtanuclear region and the cell-cell boundary, with the latter the main driver of subsequent host cell death. Based on these results, we propose that *C. albicans* invasion damages epithelia in a sequential process in which candidalysin secretion acts to prime host membranes enveloping invading hyphae for subsequent rupture. Hyphal traversal of two distinct host subcellular niches then triggers membrane rupture, resulting in a niche-specific host response that is predictive of host cell survival or death.

Introduction

The oral, genital and intestinal mucosa of most healthy individuals are colonized by the fungal pathobiont *Candida albicans* as part of the normal commensal microflora[1]. *C. albicans* causes superficial infections such as oral or vaginal thrush, and in susceptible hosts can invade the intestinal epithelial barrier and enter the bloodstream, leading to a severe systemic infection[2]. *C. albicans* transforms from a round yeast cell to a filamentous hyphal form in response to various environmental cues, a transition that facilitates tissue invasion and subsequent host damage[3].

The first barrier encountered by *C. albicans* during infection is the host epithelium. After attachment of the yeast form to the epithelial surface, hyphal growth is initiated, followed by invasion into the epithelial layer, mainly via an intracellular (transcellular) route[4,5]. As hyphae extend, they are tightly enveloped by the plasma membrane of the invaded host cell, forming a structure known as the 'invasion pocket'[6,7]. During invasion into Caco-2 cells, a model for enterocytes, extending hyphae can expand the invasion pocket into neighboring host cells without membrane breaching, forming a multi-layered structure termed *Candida albicans* trans-cellular tunnel (CaTCT)[5]. Hyphal extension within the invasion pocket or trans-cellular tunnels ultimately results in host membrane damage, followed by host cell death and epithelial layer degradation[4]. Hyphal extension *per se* is thought to cause little or no host damage despite the extensive remodeling of invasion pocket membranes during invasion[6,8]. Instead, damage is dependent on candidalysin, a secreted fungal peptide toxin encoded by the gene *ECE1*, that targets host glycosaminoglycans and induces the formation of pores within host membranes[6,9,10]. *C. albicans* strains that do not express candidalysin adhere and invade normally, but are unable to damage host cells[6,7]. As the exogenous addition of synthetic candidalysin peptide directly to host cells results in significantly less damage compared to that observed during *C. albicans* hyphal invasion (unless extremely high peptide concentrations are used), it is thought that both candidalysin secretion and hyphal invasion are required for *C. albicans* to induce its full damage potential[6,7,11]. Mogavero et al. have shown using anti-candidalysin llama V_HHs (nanobodies) that during infection of oral epithelial cells, candidalysin is secreted within the invasion pocket[7]. They go on to propose that candidalysin accumulation within the invasion pocket allows the toxin to reach a concentration sufficient for host membrane damage, thus explaining the observed difference in damage between exogenously added candidalysin and hyphal invasion. Additionally, Moyes et al. have reported that different concentrations of exogenously added candidalysin induce differential host responses in epithelial cells: signal transduction through MAPK, p38/MKP-1 and c-Fos, resulting in the production of immune cytokines by sub-lytic toxin concentrations, and a calcium influx resulting in the release of damage associated cytokines by lytic toxin concentrations[6]. Thus, it was proposed that candidalysin has dual functionality in a concentration-dependent manner, and that during infection, it is candidalysin accumulation within the invasion pocket that drives a matching dual innate immune response: pathogen recognition before appreciable host membrane damage, followed by a host response to membrane damage[6,12].

Current understanding of *C. albicans* epithelial invasion and damage is based mostly on end-point microscopy following fixation as well as population-level damage assays such as LDH release[4,11,13]. While highly informative, such approaches are limited in their ability to assess the dynamics and precise spatial organization of these processes. In this work we explore the interplay between epithelial invasion, damage and candidalysin secretion using an *in vitro* epithelial infection model and live cell imaging in combination with real-time host cell damage-sensitive reporters[5]. Our approach allows for direct, single-cell level quantitative investigation of *C. albicans* epithelial infection at distinct spatial and temporal

scales. We begin by analysis of the global dynamics of host membrane rupture and cell death using a *C. albicans* wild-type strain and a mutant strain that does not express candidalysin (*ece1Δ/Δ)*. We go on to describe the three-dimensional architecture of invasion and the different spatial organizations of host membrane rupture. Finally, we demonstrate that membrane rupture occurs at distinct host subcellular niches, each associated with specific structural and functional features. Based on these results, we propose a new model for the sequential infliction of damage by *C. albicans* during epithelial infection and discuss how it relates to existing models in the field.

Results

Single-cell level quantitative analysis of *C. albicans* invasion and damage using live cell imaging combined with damage-sensitive reporters.

In order to track the dynamics and spatial organization of *C. albicans* invasion and damage at the single-cell level, we have established an *in vitro* epithelial infection model for quantitatively monitoring live cell imaging in three-dimensions using damage-sensitive reporters (see **Figure 1A**). TR146 oral epithelial cells, widely used to study *C. albicans* infection[6,9,14,15], were engineered to express the damage-sensitive reporter Galectin-3 linked to the fluorescent reporter mOrange[5,16,17]. Galectin-3 is a small soluble protein localized to the cytosol, which binds β-galactose-containing carbohydrates typically found on the luminal side of intracellular vesicles and at the outer leaflet of the plasma membrane. By tracking mOrange-Galectin-3 (hence referred to as Gal-3), the location and spatial organization of membrane rupture events can be identified in real-time, as once a host membrane is breached, cytosolic Gal-3 flows through the rupture site and onto the cell surface where it remains bound. This approach enables the detection of significant membrane damage generally considered 'catastrophic', but is incapable of detecting smaller, 'non-catastrophic' rupture events such as those induced by bacterial toxins[18,19]. Following seeding in a microplate (96-well plate), confluent epithelial cells are stained with CellMask Deep Red (CM), which labels the host plasma membrane and endocytic compartment, including *C. albicans* induced 'invasion pockets', but not *C. albicans* membranes[5]. Host cells are also stained with SYTOX green (SYTOX), a nucleic acid stain that is impermeant to live cells but marks the nucleus of dead cells. In all experiments, two *C. albicans* strains are studied in parallel (in different wells): the wild-type (WT) prototroph BWP17 and *ece1Δ/Δ*, a mutant strain that does not express the fungal toxin candidalysin[6]. [6,11,20]. A multiplicity of infection (MOI) of 0.001 (i.e. a single *C. albicans* germ cell, hence referred to as 'inoculating yeast' (IY), added for every thousand epithelial cells) is used, followed by live cell imaging for 12 hours with 10 min imaging intervals (40X objective) or 24 hours with 30 min imaging intervals (20X objective), depending on the specific experiment, followed by image analysis and quantification.

A unique feature of our experimental design is the low number (1-4) of inoculating yeast (IYs) tracked over time within a distinct 'infection site' (see **Figure 1B**). At the start of a live cell imaging experiment (t = 0), a small group of IYs bound together are identified and centered to the middle of the microscope field-of-view (FOV) so that no additional IYs are observed within the FOV.FOVs containing more than one group of IY were not acquired. As a result, all hyphae extending within the FOV as well as all subsequent 'infection events' (e.g. host membrane rupture, host cell death) over the course of an experiment can be directly associated with the number of IYs identified at time 0 This constitutes a single 'infection site' that can be analyzed in detail at the single-cell level. An additional advantage of this setup is that the low number of IYs at the start of infection makes manual and automated detection and annotation of discrete

infection events over many hours technically feasible, without quickly overcrowding the FOV. Live cell imaging is performed in parallel at multiple infection sites within each well and in multiple wells (allowing direct comparison of different conditions, such as WT and *ece1Δ/Δ* infections and uninfected controls) in four channels: Brightfield (BF), SYTOX, Gal-3 and CM (see **Figure 1C, Supplementary Movies 1 and 2**). Individual membrane rupture events are detected as transient local increases in Gal-3 signal (termed 'Gal-3 recruitments') along the trajectories of extending hyphae (see **Figure 1C inset**).

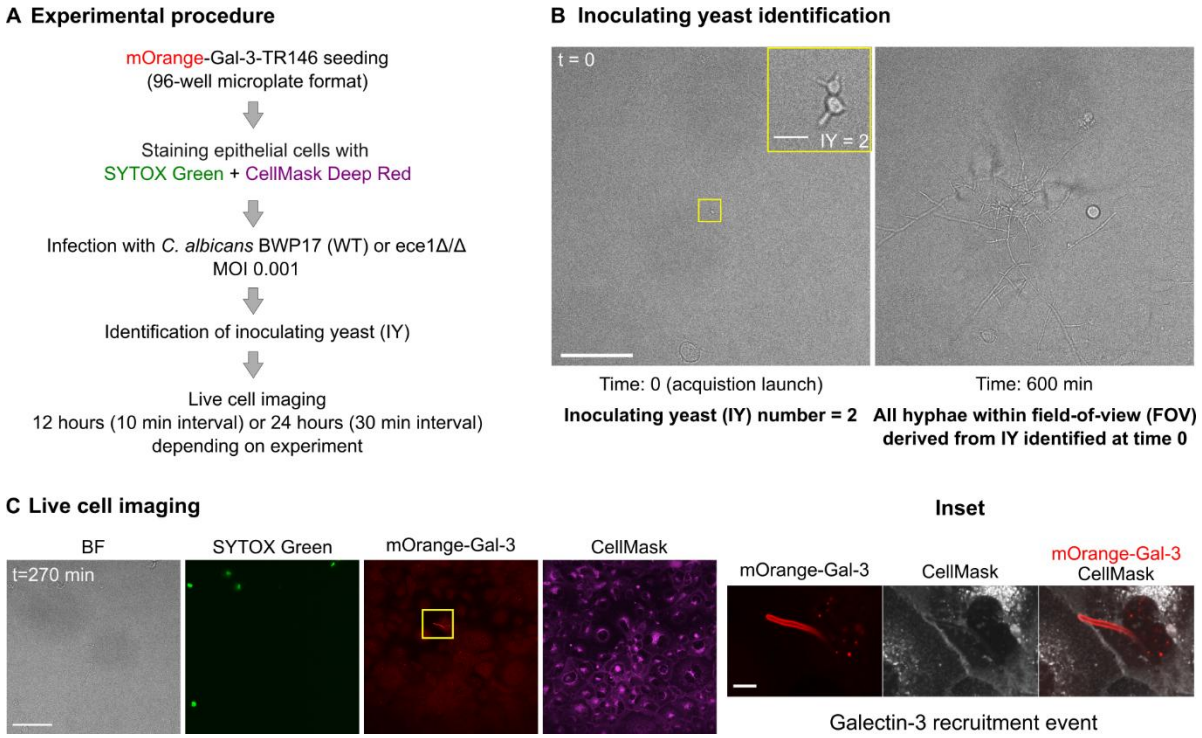

Figure 1. Single-cell level quantitative analysis of C. albicans invasion and damage using live cell imaging combined with damage-sensitive reporters. *(A) confluent TR146 cells expressing mOrange-Galectin-3 plated in a microplate are stained with the host membrane marker CellMask Deep Red and the cell death marker SYTOX green, followed by the addition of C. albicans. wildtype and ece1Δ/Δ strains at a MOI (multiplicity of infection) of 0.001. Inoculating yeast (IY) identification is followed by live cell imaging for either 12 hours with 10 min intervals or 24 hours with 30 min intervals, depending on the experiment. (B) At the start of infection (t = 0), sites containing between one and four IYs are identified and centered to the middle of the microscope field of view (FOV), followed by live cell imaging of multiple FOVs in parallel. All subsequent infection events (e.g. membrane rupture, host cell death) observed are derived from the identified IY at time 0, comprising a single 'infection site'. (C) Live cell imaging in four channels allows recording of IY and surface hyphal extension (brightfield channel, BF), host cell death (SYTOX green), host membrane rupture (mOrange-Gal-3) and host membrane organization including invasion pockets induced by C. albicans hyphae (CellMask). Individual Galectin-3 recruitment events are detected as transient increases in signal along the hyphal trajectory (Inset). Scale bars are 100 µm or 10 µm in inset. See also* ***Supplementary Movies 1 and 2 for examples of 12- and 24-hours acquisitions****.*

Fungal load is inversely proportional to individual inoculating yeast damage potential

We first studied the dynamics of host membrane rupture during the first 12 hours of WT and *ece1Δ/Δ* infection (**see Figure 2**). Multiple infection sites containing between 1 and 4 IY were imaged every 10 minutes, with individual galectin-3 recruitment events recorded at each time point in four independent experiments (see **Figure 2A, Supplementary movie 1**). Quantification of Gal-3 recruitments was stopped after 10 hours, as past this point infection sites became very crowded resulting in ambiguity in Gal-3 recruitment identification and classification. As expected, during WT infection, total Gal-3 recruitments increased over time, with a lag time of around 200 minutes from the start of infection. During *ece1Δ/Δ* infection, hyphae invaded normally, while total Gal-3 recruitments remained low but did show a slight increase over time. Plotting the total number of Gal-3 recruitments at 10 hours of infection against the IY number (see **Figure 2B**) showed a statistically significant increase in total Gal-3 recruitment as a function of IY number for the WT, but not for *ece1Δ/Δ*. Plotting the total number of Gal-3 recruitments at 10 hours divided by the IY number (representing the contribution of individual IY to total Gal-3 recruitments) against the IY number (see **Figure 2C**) showed a statistically significant inverse correlation for the WT but not for *ece1Δ/Δ*. Thus, for WT infection, the potential of individual IY to drive host membrane breaching is inversely proportional to the fungal load (i.e. IY number), a trend not observed for *ece1Δ/Δ*. This result implies the presence of inhibition or interference in damage infliction when more than one IY is present at the infection site at t = 0. The total number of WT Gal-3 recruitments recorded at 10 hours in sites with a single IY was on average 12 (n = 3). For *ece1Δ/Δ* the average for all infection sites was 1.13 (IY = 1-4, n = 23). Thus, excluding the inhibitory effect of the fungal load in WT infection sites with IY > 1, our analysis shows that WT infection results in around ten times more membrane breaching events compared to *ece1Δ/Δ* infection.

Next, we performed an equivalent analysis on the number of host cell deaths as indicated by individual SYTOX green labeling events during a 24-hour infection using WT, and *ece1Δ/Δ* strains (IY range 1-4) as well as non-infected control (NI) in three independent experiments (see **Figure 2D, Supplementary movie 2**). During WT infection, host cell death increased over time, with a lag time of around 10 hours from the start of infection. During *ece1Δ/Δ* infection, total host cell death remained low, but did show a slight increase over time, a trend also observed in the non-infected control. Plotting the total number of host cell deaths at 24 hours of infection against the IY number (see **Figure 2E**) showed an increase in total host cell deaths as a function of IY number for the WT, though it was not statistically significant. Infection with *ece1Δ/Δ* and the non-infected control did not show an increase correlated to IY number. Plotting of the total number of host cell deaths at 24 hours divided by the IY number (representing the contribution of individual IY to total host cell death) against the IY number (see **Figure 2F**) showed an inverse correlation trend for the WT (though not statistically significant, ANOVA p value = 0.064) but not for *ece1Δ/Δ*. Taken together, for WT infection, the fungal load (i.e. IY number) is inversely proportional to the potential of individual IY to drive host cell death, a trend not observed for *ece1Δ/Δ*. Mirroring our quantification of Gal-3 recruitment events, here too our results suggest the presence of inhibition or interference in damage infliction when more than one IY is present at the infection site at t = 0. As host membrane rupture and host cell death are mechanistically linked (i.e. host membrane rupture drives host cell death, see below), it is likely that the proportionality we observe for Gal-3 recruitment and host cell death are derived from the same inhibitory mechanism. The total number of WT host cell death recorded at 24 hours in sites with a single IY was on average 113 (n = 3). For *ece1Δ/Δ* the average for all infection sites was 25 (IY = 1-4, n = 15) and for the non-infected control 20 (n = 11). As the values of total host cell death at 24 hours

during *ece1Δ/Δ* infection are comparable to the non-infected control, *ece1Δ/Δ* infection appears to result in little or no additional host cell death in our system. Excluding the inhibitory effect of the fungal load in WT infection sites with IY > 1, WT infection results in around five times more host cell deaths compared to non-infected cells or cells infected with *ece1Δ/Δ*.

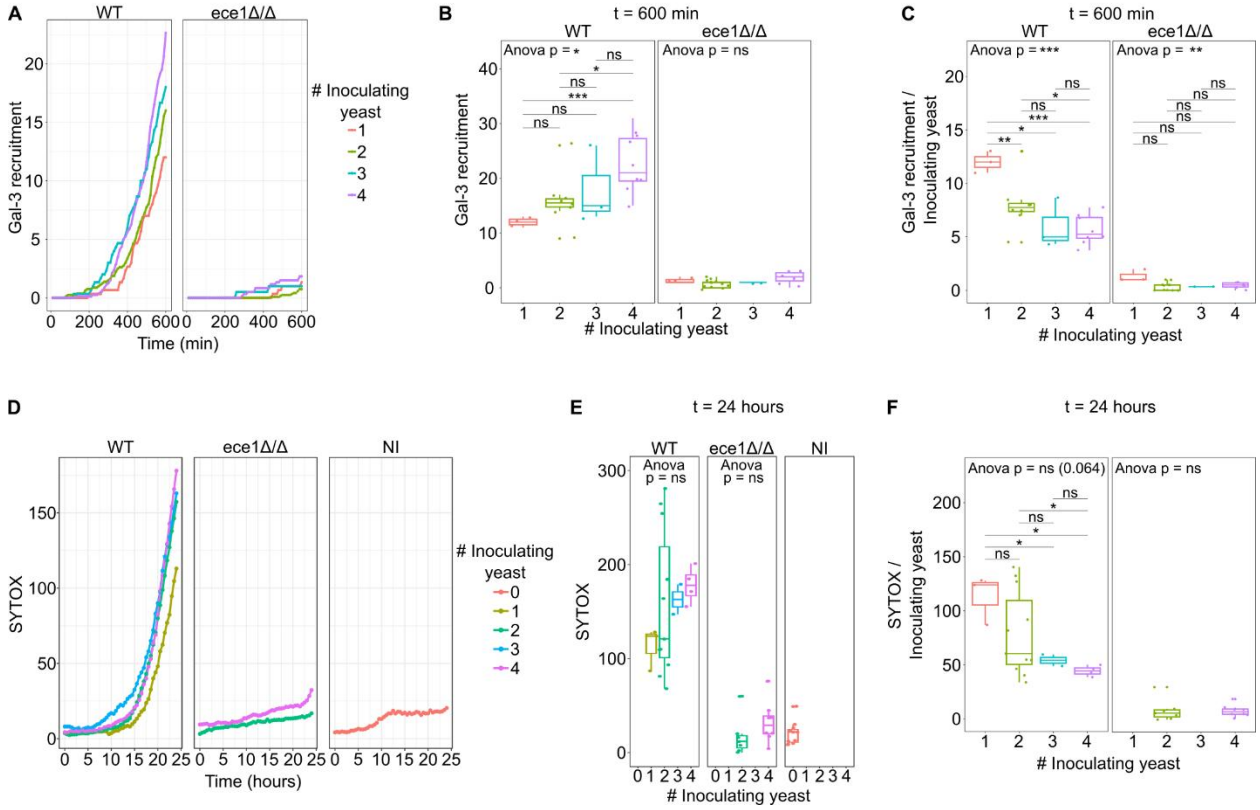

Figure 2. Fungal load is inversely proportional to individual IY damage potential. *(A) Total host membrane rupture as indicated by galectin-3 recruitment events during the first 10 hours of infection using WT and ece1Δ/Δ strains. Images were acquired every 10 min, and each individual Gal-3 recruitment event was recorded over time. (B) Total Gal-3 recruitments at 10 hours of infection plotted against the inoculating yeast (IY) number. (C) Total Gal-3 recruitments events at 10 hours divided by inoculating yeast number plotted against the inoculating yeast number, representing the contribution of individual inoculating yeast to total Gal-3 recruitments. (D) Total host cell deaths as indicated by SYTOX green labeling during a 24-hour infection using WT and ece1Δ/Δ strains. No-infected (NI) wells are presented as a control. Images were acquired every 30 minutes and each individual SYTOX green labeling event was recorded over time. (E) Total host cell deaths at 24 hours of infection plotted against the inoculating yeast number. (F) Total host cell deaths at 24 hours divided by inoculating yeast number plotted against the inoculating yeast number, representing the contribution of individual inoculating yeast to total host cell deaths. Representative acquisitions used for data collection and analysis are presented in* ***Supplementary Movie 1*** *(12-hour acquisition) and* ***Supplementary Movie 2*** *(24-hour acquisition).*

Apical invasion is succeeded by hyphal extension within a partial basolateral invasion pocket

Following our global analysis of host membrane rupture and cell death during infection, we turned to examine the nature of hyphal extension and damage in detail. Examination of three-dimensional trajectories of invading hyphae revealed the following sequence (see **Figure 3A, B Supplementary movie 3**): after the yeast-to-hypha transition, hyphae extend along the epithelial layer surface; the first invasion is initiated at the host apical membrane; hyphae then traverse the first host cell and arrive at the microplate surface (i.e. base of the imaging well) followed by host membrane rupture (as indicated by Gal-3 recruitment) within the same cell; from this point onwards, hyphae extend along the microplate surface below the basolateral side of epithelial cells for the remainder of infection,i.e. only invading 'basolaterally'. High-resolution imaging of invasion pockets formed by basolaterally invading hyphae revealed that hyphae indent the host basolateral membrane forming a 'partial invasion pocket', which does not fully envelop the hyphae on all sides (see **Figure 3C**). Based on measurements of the invasion pocket geometry (see **Supplementary Figure S1**) and modeling the invasion pocket cross-section as a perfect circle with a base at the microplate surface, we estimate that around 87% of the hyphal circumference comes into contact with the host basolateral membrane, while 13% is in contact with the microplate surface. Taken together, our analysis shows that past the first invaded host cell, hyphae extend along the basolateral side of the epithelial monolayer throughout infection, forming 'partial invasion pockets' that indent the host basolateral membrane but do not entirely envelop invading hyphae. This 'invasion architecture' stands in contrast to a previous study of early *C. albicans* invasion into Caco-2 enterocytes monolayers, in which apically invading hyphae extended within the epithelial layer without reaching the microplate surface for hours, forming complete (i.e. fully membrane-enveloped) invasion pockets and trans-cellular tunnels in the process[5] (See **Discussion**).

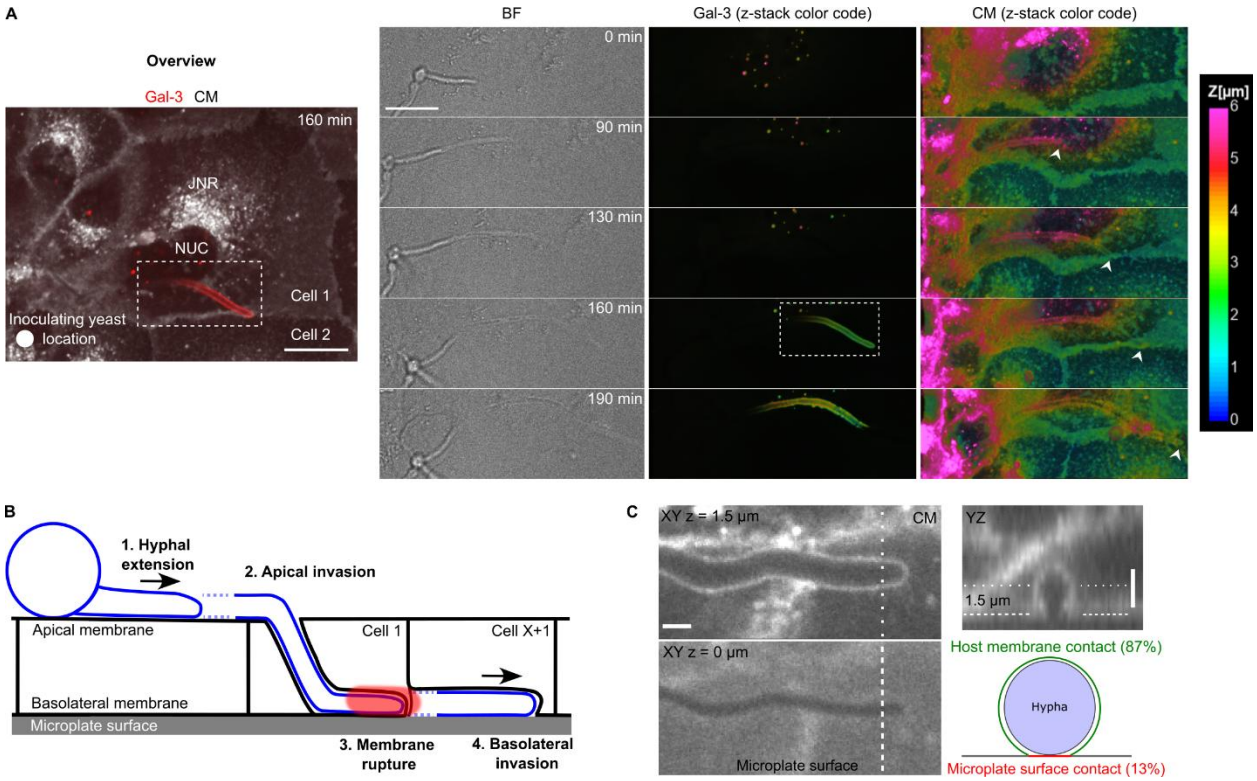

Figure 3. Apical invasion of TR146 cell monolayers is succeeded by hyphal extension within a partial basolateral invasion pocket *(A) The membrane rupture presented in Figure 1C is analyzed in detail, with the dataset now oriented such that the microplate base is at z = 0 µm and the top of the epithelial layer (apical side) is at z = 6 µm, and the invading hypha is extending from left to right. An overview shows the location of the inoculating yeast, the host nucleus (NUC), juxtanuclear region (JNR), the apically invaded cell (Cell 1), and the second basolaterally invaded cell (Cell 2) at the moment of Gal-3 recruitment. The trajectory of the hypha is presented at different time points, with the Gal-3 and CM channels presented with z-color coding. The hypha apex at different timepoints is marked with an arrow head. Invasion begins at the apical side and continues until the basolateral side (microplate surface) is reached. Gal-3 recruitment occurs at the basolateral side of Cell 1. The hypha then continues to extend along the same z into Cell 2. (B) A model showing the different steps of invasion: (1) Hyphal extension along the apical surface, (2) Apical invasion, (3) Membrane rupture in the apically invaded cell (4) Basolateral invasion in all subsequently invaded cells. (C) High-resolution analysis of the invasion pocket geometry during basolateral invasion. Two z-sections show the hypha at maximum diameter (z = 1.5 µm) and in contact with the microplate surface (z = 0 µm) in an XY view. A YZ view shows the invasion pocket membrane remains 'partially open' to the microplate surface. Lines indicate source of cross-sectional views. Measurements of invasion pocket diameter (see* ***Supplementary figure S1****) and modeling the invasion pocket cross-section as a perfect circle with a base at the microplate surface, we estimate that 87% of the hyphal circumference comes into contact with the host basolateral membrane (green), while 13% is in contact with the microplate surface (red). Scale bars are 100 µm in the overview and 10 µm in timeline in (A) and 2 µm in (C). See also* ***Supplementary movie 3****.*

Gal-3 recruitment patterns are regulated by candidalysin and are predictive of host cell death

Next, we examined the spatial organization of host membrane rupture sites, their regulation by candidalysin and correlation with host cell death (see **Figure 4**). Analysis of Gal-3 recruitment patterns observed during the first 10 hours of infection in three independent experiments revealed that patterns can be classified into three distinct categories that are not temporally linked (i.e. one pattern does not transition into another over time) (see **Figure 4A, Supplementary movies 4, 5, 6**): 'tip' recruitment, defined by Gal-3 recruitment in a small region at the invasion pocket tip (i.e. near the hyphal apex), 'tubular' recruitment, defined by Gal-3 recruitment along a short section of the 'neck' of the invasion pocket, excluding the invasion pocket tip, and 'elongated' recruitment, defined by a long Gal-3 recruitment along the invasion pocket length that includes both the tip and the neck. Quantification of the distribution of recruitment patterns during infection revealed that for the WT strain, 'tip' recruitment is observed in 66.8% of all events, 'tubular' in 19.6%, and 'elongated' in 13.6% (n = 404). For *ece1Δ/Δ*, all events occurred in the 'tip' recruitment pattern (n = 23) (see **Figure 4B**). Taken together, membrane rupture occurs with three distinct spatial organizations, two of which are dependent on the presence of candidalysin ('tubular' and 'elongated'), and one observed with or without the presence of candidalysin ('tip'). Past the first 10 hours of infection, infection sites became very crowded, making unambiguous determination of Gal-3 recruitment patterns difficult. Furthermore, from this point on, Gal-3 recruitments resulting from hypha-hypha collisions became increasingly abundant, likely driven by the invasion architecture of our experimental model in which all hyphae extend along the microplate surface after the first apical invasion (see **Discussion).**

Next, we analyzed the correlation between the three Gal-3 recruitment patterns and host cell death as indicated by SYTOX labelling. An individual galectin-3 recruitment pattern was considered correlated to host cell death if a subsequent SYTOX signal was observed within one hour (six acquisition intervals) in the same cell in which Gal-3 recruitment was initially observed. In three independent experiments we found that for the WT strain, 'tip' recruitment was correlated to host cell death in 8% of events (n = 21/270), 'tubular' recruitment in 30.5% of events (n = 24/79) and 'elongated' recruitment in 72% of events (n = 41/55) (see **Figure 4C**). During infection with the *ece1Δ/Δ* strain, we did not observe any host cell death following Gal-3 recruitment (n = 23). These results suggest that candidalysin-dependent Gal-3 recruitment patterns (i.e., observed only during WT infection) are linked to increased cell death compared to the 'tip' recruitment pattern, observed in both WT and *ece1Δ/Δ* infections. We hypothesize that the 'elongated' recruitment pattern, which is largely concurrent with SYTOX labeling, is likely a result of general host cell membrane permeabilization during cell death, leading to Gal-3 recruitment along the invasion pocket membrane, a phenomenon previously observed also during *C. albicans* HeLa cell invasion[5]. Overall, our results indicate that rupture site spatial organization is predictive of host cell death in a candidalysin-dependent manner, with recruitment patterns observed only in the presence of candidalysin ('tubular' and 'elongated'), showing higher correlation to host cell death compared to the recruitment pattern observed in both the WT and *ece1Δ/Δ* strains ('tip').

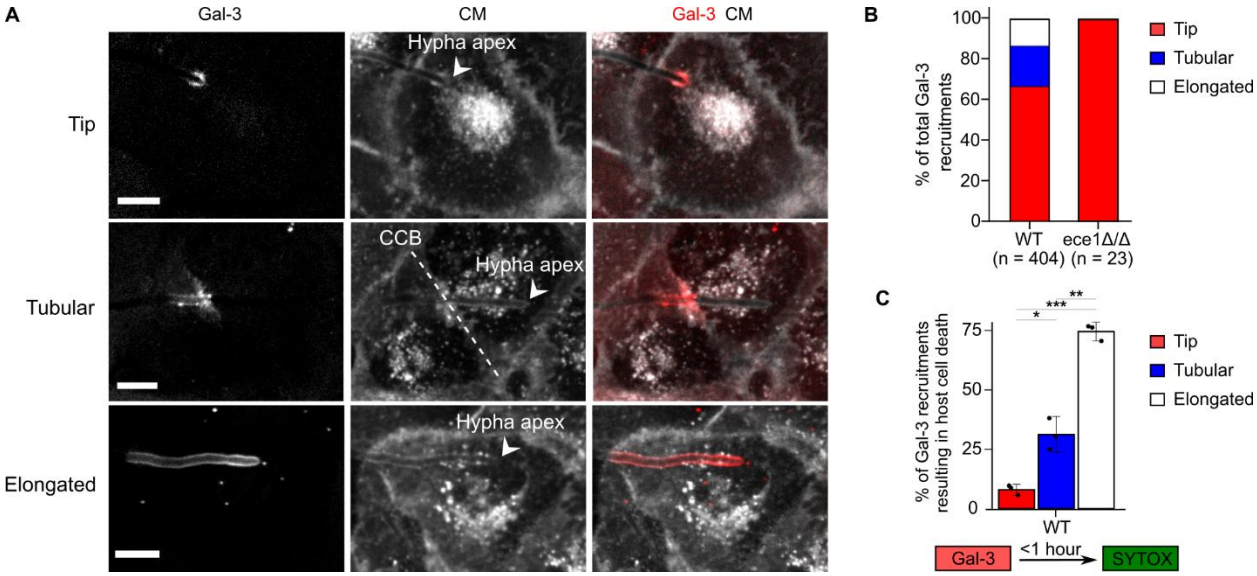

Figure 4. Galectin-3 recruitment patterns are regulated by candidalysin and are predictive of host cell death. *(A) Galectin-3 recruitment patterns were classified into three categories: 'tip', 'tubular' and 'elongated'. The hypha apex (arrowheads) and cell-cell boundary (CCB, dotted line) are indicated. (B) Distribution of recruitment patterns during WT and ece1Δ/Δ infection (n=404 WT and n=23 ece1Δ/Δ Gal-3 recruitments from three independent experiments). (C) Correlation between Gal-3 recruitment pattern and host cell death. Gal-3 recruitment was considered correlated to host cell death if a SYTOX signal was observed within the same cell up to one hour after Gal-3 recruitment. As no host cell death was observed during infection with the ece1Δ/Δ strain, only WT data is shown (n = 86 SYTOX labeling events following 404 Gal-3 recruitment events in three independent experiments). Scale bars are 10 µm. See also Supplementary movies 4, 5, 6.*

Host membrane rupture occurs at two distinct host subcellular niches: the juxtanuclear region and the cell-cell boundary

Our detailed analysis of Gal-3 recruitment dynamics and spatial organization led to the surprising observation that the location of Gal-3 recruitments within host cells is associated with two specific host subcellular niches: the juxtanuclear region and the cell-cell boundary. This phenomenon is illustrated using a high-temporal and -spatial resolution acquisition of a two-hour WT infection window with imaging intervals of two minutes using the Gal-3 and CM channels (see **Figure 5A, Supplementary movie 7**). The typical invasion path of a single hypha extending through two host cells over the course of around 90 minutes is presented in an overview: at time = 0, the invading hypha is already enveloped in a 'partial invasion pocket'; first the hypha extends in proximity to the vesicle rich juxtanuclear region in cell one (JNR1); the hypha then extends pass the cell-cell boundary (CCB) separating the two host cells; and finally the hypha extends near the juxtanuclear region of cell two (JNR2). Gal-3 recruitment events occur several times along the path of invasion, with the first event occurring in proximity to JNR1 (R1), followed by a rupture at the CCB (R2), and finally in proximity to JNR2 (R3). Insets show the spatial organization of each recruitment event, with 'tip' recruitment for R1 and R3 and 'tubular' recruitment for R2.

Quantitative analysis was performed via manual annotation of the location of each Gal-3 recruitment event observed during three independent 12-hour infection acquisitions using both WT and *ece1Δ/Δ* strains (n = 351 WT and n = 21 *ece1Δ/Δ*). Locations were classified into three categories: recruitment at the CCB, recruitment in proximity to the JNR, and recruitment at the cytoplasm (i.e., without proximity to the JNR or CCB) (see **Figure 5B**). As 'elongated' Gal-3 recruitment patterns (accounting for 13.6% of all recruitment events) span the length of most of the host cell, their location could not be classified unambiguously, and thus they were omitted from the location analysis. For the WT strain, 47% of Gal-3 recruitment events occurred at the CCB, 49% at the JNR, and 4% at the cytoplasm. For the *ece1Δ/Δ* strain 48% of Gal-3 recruitment events occurred at the CCB, 38% at the JNR, and 14% of events in the cytoplasm. The distribution of locations between the two strains was not statistically different. As a reference, we estimate that the cytoplasm (including the area between the basolateral membrane and the base of the nucleus) occupies around 87% of the cell area on the basolateral side of TR146 cells, compared to 13% occupied by the JNR (see **Supplementary Figure S2**). Taken together, our results suggest that host membrane rupture occurs predominantly at two distinct host subcellular niches: the CCB and the JNR, and that membrane rupture location is not regulated by candidalysin.

Membrane rupture at the cell-cell boundary is the main driver of host cell death

Next, we combined the Gal-3 recruitment pattern analysis (see **Figure 4B**) with the Gal-3 recruitment location analysis (see **Figure 5B**), assigning both a recruitment pattern and a location to WT recruitment events (n= 351 Gal-3 recruitments, 'elongated' recruitment pattern excluded, see above) as 'pattern-location' pairs (see **Figure 5C**). *ece1Δ/Δ* infection was not analyzed as all recruitments occurred with the 'tip' pattern. Our results revealed several interesting trends: almost half of all recruitment events (49%) occurred as 'tip-JNR', whereas 'tubular-JNR' pairs were never observed. In other words, only 'tip' recruitments were observed at the JNR region. Tubular recruitments occurred almost exclusively at the CCB (79/80 total tubular Gal-3 recruitments), suggesting this recruitment pattern is strongly associated with hyphae traversing the cell-cell boundary. 'Tip' and 'tubular' recruitments at the CCB occurred in approximately equal proportions (24.5% and 22.5% respectively).

Finally, WT 'pattern-location' pairs were correlated with subsequent host cell death (SYTOX signal appearing within one hour of Gal-3 recruitment in the same cell, see **Figure 4C**). Overall, 13% of total Gal-3 recruitments events ('elongated' pattern excluded) resulted in host cell death within one hour (n=45/351). Within this subset (n=45), 53.3% of host cell deaths occurred following 'tubular-CCB' Gal-3 recruitment. As 'tubular-CCB' recruitments account for only 22.5% of all Gal-3 recruitment (see **Figure 5C**), we conclude that the 'tubular-CCB' pair is strongly correlated with host cell death. In contrast, 31.1% of host cell deaths occurred following 'tip-JNR' Gal-3 recruitment, while accounting for 49% of all total Gal-3 recruitment events. Thus, we conclude that the 'tip-JNR' pair is weakly correlated to host cell death. Comparing the correlation between Gal-3 recruitment location and host cell death (irrespective of the recruitment pattern) reveals that while the proportion of JNR and CCB Gal-3 recruitments events is nearly identical (49% to 47% respectively, see **Figure 5C**), CCB recruitments are correlated to 66.6% of total host cell death, versus only 31.1% of events in the JNR. Taken together, Gal-3 recruitments at the CCB, and in particular those associated with the 'tubular' recruitment pattern, are strongly correlated to subsequent host cell death, suggesting membrane rupture at the CCB is the main driver of subsequent infection damage. In contrast, membrane rupture at the JNR (associated exclusively with 'tip' recruitment pattern) is weakly correlated to host cell death, suggesting this subcellular niche is relatively non-damaging, and plays a smaller role in generating long-term infection damage.

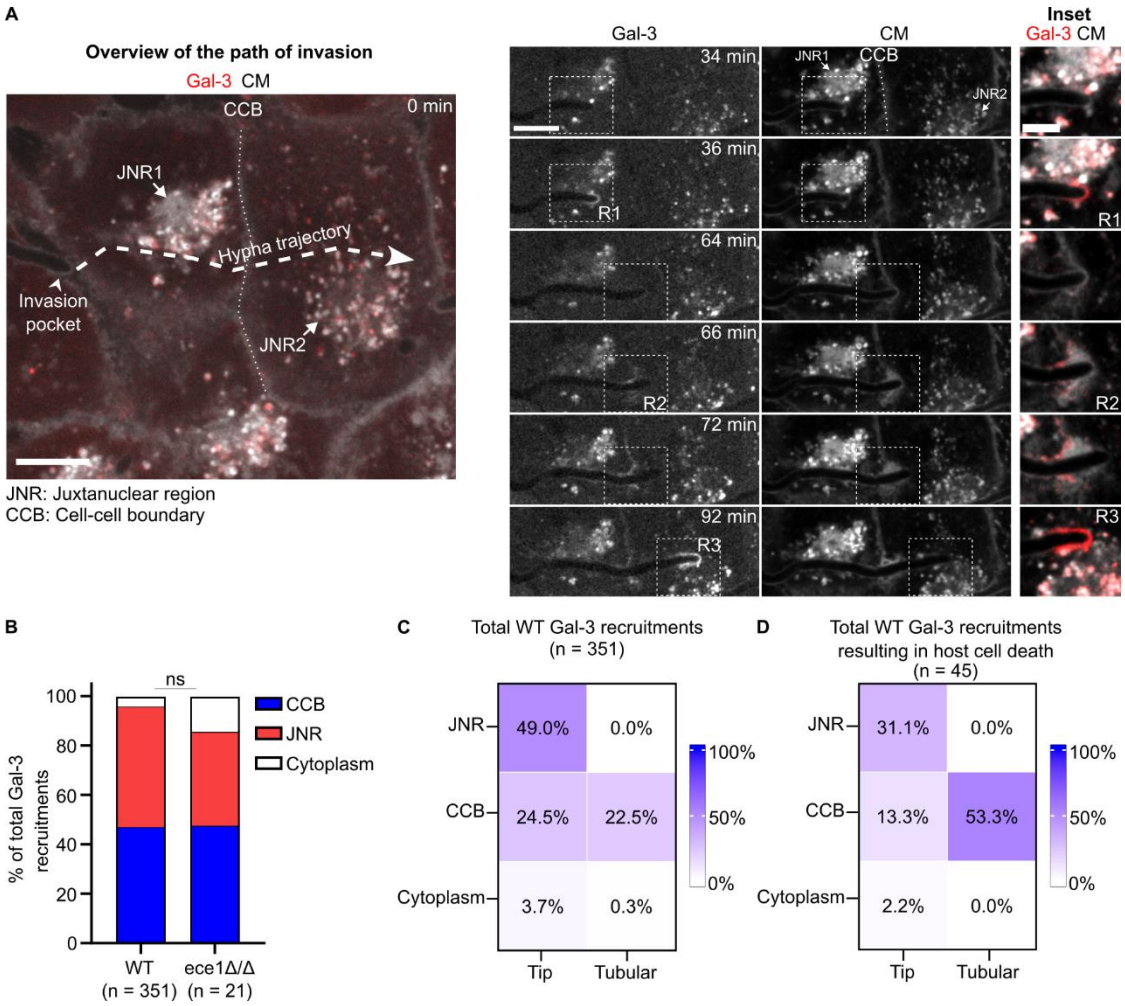

Figure 5. Galectin-3 recruitment occurs at distinct host subcellular niches: the juxtanuclear region (JNR) and cell-cell boundary (CCB). *(A) High temporal- and spatial-resolution live cell imaging showing multiple galectin-3 recruitment events occurring along the invasion path of a single hypha invading several host cells in sequence. An overview of the hypha trajectory starting at 0 min is presented. A 'partial invasion pocket' is already present at t = 0 (arrowhead). The hypha trajectory traverses the juxtanuclear region of cell one (JNR1), the cell-cell boundary (CCB) and the juxtanuclear region of cell two (JNR2). A detailed view of Gal-3 recruitments occurring at JNR1 (R1), the CCB (R2), and the JNR2 (R3) is presented, with insets showing a magnified view. Imaging was performed for 2 hours with 2 minutes intervals. (B) Quantification of Gal-3 recruitment location, classified into three categories: cell-cell boundary (CCB), juxtanuclear region (JNR) and cytoplasm. Analysis is based on 12-hour infection acquisitions with an imaging interval of 10 min from three independent experiments (n=351 WT and n=21 ece1Δ/Δ Gal-3 recruitments). The difference in galectin-3 recruitment locations between WT and ece1Δ/Δ infections is not statistically significant. (C) Distribution of WT Gal-3 recruitment* 'pattern-location' pairs *(n = 351 Gal-3 recruitments in three independent experiments. χ2 test p-value ***) (D) Distribution of WT Gal-3 recruitment* 'pattern-location' pairs resulting in host cell death (*n= 45 Gal-3 recruitments resulting in host cell death, indicated by SYTOX*

*labeling within 1 hour of Gal-3 recruitment, χ2 test p-value ***). Scale bars are 10 µm and 5 µm in inset. See also* ***Supplementary movie 7****.*

High temporal- and -spatial resolution imaging of membrane rupture reveals niche-specific features.

To obtain finer temporal and structural information about the nature of membrane rupture in each subcellular niche, we employed high temporal- and spatial-resolution live cell imaging of a two-hour infection window when Gal-3 recruitments were abundant (see **Figure 6**). A typical 'tubular/CCB' Gal-3 recruitment event is presented in detail (see **Figure 6A, Supplementary movie 8**): at the start of the timeline (0 min), a hypha enveloped by a partial invasion pocket has already extended past the length of the first cell (Cell 1) with the hypha apex at the CCB. In the next minutes (8, 16 min) the hypha extends into the second cell (Cell 2). Next, as the hypha continues to extend, a tubular Gal-3 recruitment appears (24 min). Notably, Gal-3 recruitment in the tubular pattern is observed only within the first invaded cell. Gal-3 labelling is also observed in a small section of the membrane orthogonal to the invasion pocket, suggesting damage is not limited to the invasion pocket membrane. Finally, hyphal extension within a partial invasion pocket continues in Cell 2. Overall, our high temporal- and spatial-resolution data suggest upon arrival at the CCB, hyphae 'push' the partial invasion pocket membrane formed in the first invaded cell into the second invaded cell, until a 'critical point' is reached when membrane rupture occurs selectively in the first invaded cell only (see **Discussion**). This 'cell selective' CCB recruitment pattern was commonly observed (see also **Figure 4A** and **Figure 5A**, for additional examples).

Next, we examined Gal-3 recruitment patterns associated with JNR rupture in detail. A typical 'tip/JNR' Gal-3 recruitment is presented in **Figure 6B** (see also **Supplementary movie 9**). The first time point in which Gal-3 recruitment is observed shows a typical 'tip' recruitment pattern. Closer examination of this structure suggests the presence of two vesicle-like structures at the hypha apex, that are seen connected to the rest of the invasion pocket membrane (2 min). Next, several vesicles labelled with Gal-3 'pinch off' the enveloping membrane but remain close to it (4 min). A single vesicle moves away from the invasion pocket membrane, but remains tethered to it via a thin membrane connection (6 min) at which point it is 'pulled back' (8, 10, 12 min). As the hypha and invasion pocket continue to extend, Gal-3 positive vesicles are 'left behind' and remain in a static location (12, 14 min). The formation and 'removal' of Gal-3 positive vesicles were commonly observed at JNR membrane rupture sites, suggesting it is a 'niche-specific' feature. While in this study we did not attempt to further characterize the precise nature of these vesicles, our observations are in good agreement with a previous study of *C. albicans* TR146 cell infection that demonstrated the presence of membrane-derived blebs at sites of membrane rupture, suggested to be part of a specific host membrane repair response to *C. albicans* invasion (see **Discussion**)[14].

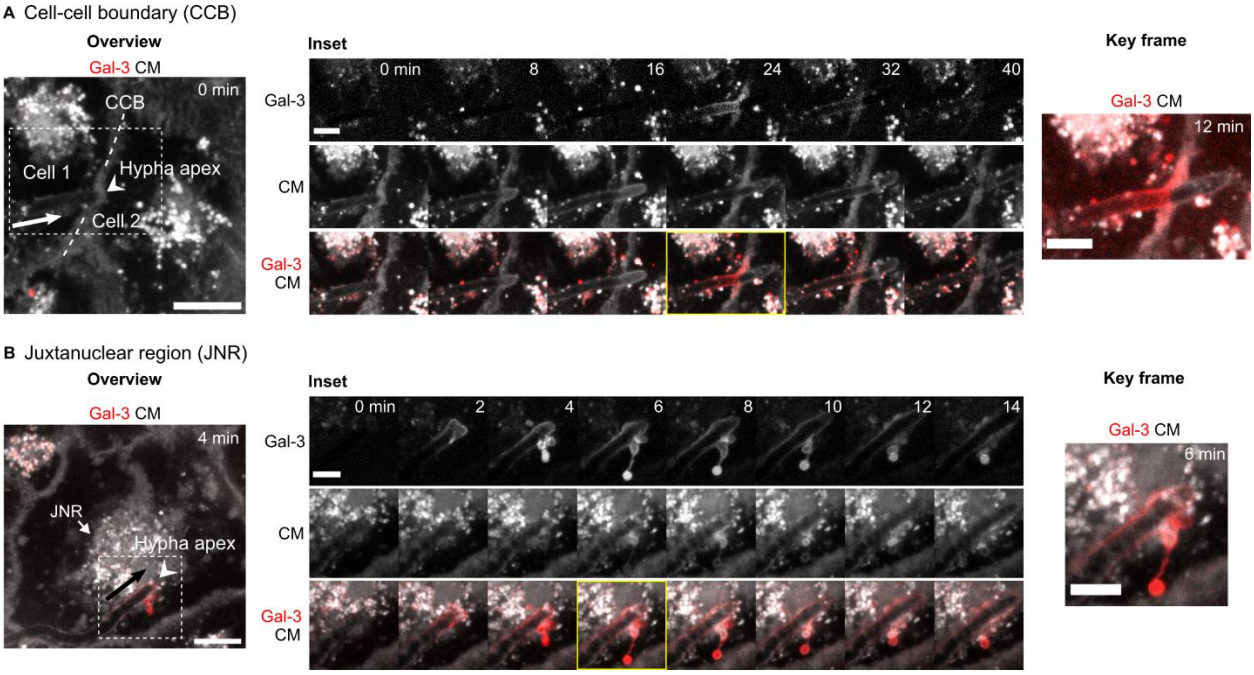

Figure 6. High temporal- and -spatial resolution imaging of membrane rupture reveals niche-specific features. *(A) 'tubular/CCB' Gal-3 recruitment. An overview shows the partial invasion pocket membrane at the CCB between cell 1 and cell 2 at t = 0 min. The hypha apex is indicated (arrowhead). The direction of extension is noted with an arrow. Inset (from dotted frame) shows the invasion pocket continues to extend into cell 2 (t = 8, 16 min). At t = 24 min, a tubular Gal-3 recruitment limited to cell 1 is observed. The invasion pocket continues to extend into cell 2 (t = 32, 40 min). A key frame (yellow) highlights 'cell selective' Gal-3 recruitment. (B) 'tip/JNR' Gal-3 recruitment. An overview shows a partial invasion pocket in close proximity to the JNR. The hypha apex is indicated (arrowhead). The direction of extension is noted with an arrow. Inset (from dotted frame) shows Gal-3 tip recruitment associated with tip two vesicle-like structures (t = 2). Next, three Gal-3 labeled vesicles are observed, with a single vesicle moving away from the invasion pocket membrane, but remains tethered to it via a thin membrane connection (6 min). It is then 'pulled back' towards the invasion pocket (8, 10, 12 min). Gal-3 positive vesicles are 'left behind' and remain in a static location in relation to the invasion pocket which continues to extend (12, 14 min). A key frame (yellow) highlights the Gal-3 positive vesicle and tether. Scale bars are 10 µm in overviews and 5 µm in insets and key frames. See also Supplementary movies 8, 9.*

Discussion

We employed live cell imaging combined with damage-sensitive reporters at different temporal- and spatial resolutions to study the interplay between hyphal extension, candidalysin secretion, and host damage during epithelial invasion by *C. albicans*. We show that the damage potential of individual inoculating yeast is inversely proportional to their number at the start of infection, and quantify candidalysin-induced damage at the single-cell level. Next, we determine the 'invasion architecture' in our experimental model showing that following an initial apical invasion, hyphae extend along the microplate surface enveloped by a basolateral 'partial invasion pocket'. We go on to show that membrane rupture is spatially organized in three distinct patterns, two of which ('tubular' and 'elongated') are dependent on the presence of candidalysin and are correlated to subsequent host cell death. Strikingly, we observe that membrane rupture occurs almost exclusively at two host subcellular niches: the cell-cell boundary (CCB) and the juxtanuclear region (JNR), and that this distribution is candidalysin-independent. Our analysis also reveals that rupture spatial organization, location and subsequent host cell death are linked, with 'tip' recruitments that are abundant in the JNR region and is weakly correlated to subsequent host cell death, while 'tubular' recruitments are abundant at the CCB and are strongly correlated to subsequent host cell death. Finally, a high-resolution analysis of membrane rupture at the CCB and JNR reveals different 'niche-specific' features.

Our analysis of infection damage measured by Gal-3 recruitment and SYTOX green labelling revealed an inverse correlation between the number of inoculating yeasts and the damage inflicted by each inoculating yeast. In other words, two inoculating yeasts inflict less than double the damage of a single inoculating yeast, a result suggestive of an inhibitory mechanism when more than one inoculating yeast is present in the same infection site. Inhibition may be due to a 'crowding effect' limiting the expansion of hyphal networks growing in close proximity, though further research is required to examine these and other possibilities. As the number of inoculating yeasts plays a role in determining the level of host damage inflicted by a single yeast, comparing damage inflicted by different *C. albicans* strains at the single-cell level in our system requires knowledge of the inoculating yeast number at each infection site. Previous studies have compared host damage inflicted by WT and *ece1Δ/Δ* strains in different models, providing an indication of the relative 'contribution' of candidalysin to total infection damage[11,20]. LDH release assays of TR146 cells after 24 hours of infection showed approximately 8-fold decrease in damage when using the *ece1Δ/Δ* strain compared to the WT strain[6]. This result is in general agreement with our study, which indicates a 10-fold decrease in host membrane breaching at 10 hours of infection (IY = 1) and a five-fold decrease in host cell death at 24 hours of infection (IY = 1) when using the *ece1Δ/Δ* strain compared to the WT strain.

We show that *C. albicans* invasion and damage in our epithelial monolayer model occurs via a specific 'invasion architecture' that has important implications both for the interpretation of our results, and more generally for assessing the physiological relevance of epithelial monolayer models for studying *C. albicans* invasion. Following an initial apical invasion and membrane damage, hyphae extend along the microplate surface beneath the host basolateral side for the remainder of infection. This results in the formation of a partial invasion pocket that indents the host basolateral plasma membrane without entirely enveloping the invading hypha. Thus, past the first apical invasion, the interactions between extending hyphae and epithelial cells can be considered as 'surface interactions', without significant invagination of the invasion pocket membrane towards the inner regions of host cells. This 'invasion architecture' stands in contrast to our previous study of invasion into Caco-2 monolayers, where following apical invasion, hyphae

extended within the epithelial layer without reaching the microplate surface for hours, traversing multiple host cells within trans-cellular tunnels[5]. The underlying mechanism for these differences in 'invasion architecture' remains unknown. Previous studies of *C. albicans* invasion of oral epithelial monolayers showed a near complete elimination of damage when using the *ece1Δ/Δ* strain compared to the WT, in line with results reported here [6,14]. These assays appear to indicate that invasion *per se* does not damage host cells, leading to the hypothesis that it is only the action of candidalysin that drives this process[8]. However, we show that the 'invasion architecture' in our monolayer infection model does not in fact entail extensive host membrane remodeling past the first apically invaded host cell. Instead, throughout infection, host membrane deformation is more akin to a local linear 'detachment' of host cells' basolateral membrane from the microplate surface along the path of invasion, which requires only minor remodeling of host membranes, at the scale of the hyphal diameter (around 2 µm), and thus is unlikely to generate significant damage from hyphal extension alone. Indeed, it is possible that monolayer infection models are not suitable for studying the role of invasion *per se,* i.e. the role of extensive host membrane deformation induced by extending hyphae, in generating host damage, and consequently, whether the notion that infection damage is 'decoupled' from hyphal invasion, holds firm[7,8]. Interestingly, studies of the role of candidalysin in inducing host damage *in vivo* have shown a significant decrease in damage when using the *ece1Δ/Δ* strain compared to the WT, yet damage is still observed, suggesting that invasion *per se* can cause limited host damage *in vivo*[6,21]. The invasion architecture in our model likely underlies two other observations made in this study: first, we did not observe any interactions (e.g. hyphal change of direction, membrane rupture) between invading hyphae and host nuclei, despite the latter representing the most rigid part of the cell and thus likely to counter hyphal extension. We attribute this to hyphae extending along the host basolateral side traversing 'underneath' host nuclei without direct hyphae-nuclei encounters. Second, we observed that around ten hours post-infection hyphal collisions become the dominant cause of host membrane rupture. Invasion architecture would imply that excluding apical invasions, all invading hyphae are extending along the microplate surface, therefore increasing the chances of hyphal collisions as the number and length of invading hyphae increases over time. Future *in vitro* studies of multi-layered infection models such as reconstituted epithelia[22], could be used to directly address the contribution of invasion *per se* to infection damage, as well as the roles host nuclei and hyphal collisions in shaping the invasive lifestyle of *C. albicans*.

Several studies have demonstrated that damage levels caused by the direct addition of exogenous candidalysin peptide to epithelial cells is significantly lower than damage observed during *C. albicans* infection[6,11]. Furthermore, infection with a yeast-locked *C. albicans* strain engineered to secret candidalysin also results in low levels of damage compared to filamenting cells[7]. These results point towards a requirement for hyphal invasion and candidalysin secretion to act together to inflict maximal damage during infection. To explain this requirement, it has been proposed that the invagination of the host plasma membrane into an invasion pocket by invading hyphae creates a microenvironment that facilitates candidalysin accumulation over time, until a lytic concentration of the toxin is reached enabling damage of the invasion pocket membrane[6,23]. While candidalysin has been shown to be present along the invasion pocket length, the precise mechanism driving such accumulation remains unknown[7]. The proposed 'accumulation' mechanism predicts that longer hyphae should cause more membrane damage compared to shorter hyphae, as longer hyphae allow more time for candidalysin accumulation within the invasion pocket [14]. Our study revealed that membrane rupture occurs almost exclusively when hyphae extend in proximity to JNR or traverse the CCB. While we did not directly measure the hyphal length at the time of rupture, we rarely observe (4% of total WT rupture events) membrane breaching occurring as

hyphae basolaterally traverse the host cytosol, despite this being by far the compartment with the largest area facing the basolateral membrane, which we estimate at around 87% in TR146 cells. If membrane rupture was directly dependent on hyphal length, most hyphae would statistically reach the required length for accumulation of lytic candidalysin concentrations while traversing the host cytosol, contrary to our observations. Instead, our results point towards an alternative mechanism linking hyphal invasion and candidalysin activity together, whereby in addition to candidalysin secretion, a second factor, hyphal traversal of distinct subcellular niches, is required to induce membrane rupture and long-term infection damage.

We thus propose the following 'sequential' damage mechanism to explain *C. albicans* epithelial damage in our experimental system: Infection begins with hyphal extension along the epithelial layer surface, followed by an apical invasion in which hyphae traverse the host cell reaching the basolateral side, resulting in membrane rupture (see **Figure 3**). From this point onwards, an 'invasion cycle' is repeated in each host cell (see **Figure 7**). As each hypha extends into a neighboring cell along the microplate surface, it forms a basolateral 'partial invasion pocket'. Candidalysin is secreted into the partial invasion pocket, resulting in a candidalysin-dependent 'sub-lytic' invasion pocket (see below). Next, the hypha may extend in proximity to the host JNR, where the 'sub-lytic' invasion pocket is detected by the host, followed by membrane rupture and vesicle removal, possibly as part of a host membrane repair response (see below). Eventually, the extending hypha arrives at the CCB, which acts as an orthogonal rigid barrier that can exert a counter-force against the extending hypha enveloped by a 'sub-lytic' invasion pocket (see below). CCB traversal leads to rupture of the 'sub-lytic' invasion pocket membrane, which is associated with host cell death and long-term infection damage. Finally, hyphal extension continues into a neighboring cell, where a new partial invasion pocket is formed, thus restarting the invasion cycle.

In the proposed 'sequential' damage mechanism, invading hyphae are continuously enveloped by candidalysin-dependent 'sub-lytic' partial invasion pockets. The transition from 'sub-lytic' to 'lytic' only occurs during hyphal traversal of the JNR and the CCB, due to specific niche-associated interactions. In the absence of candidalysin secretion (i.e. during infection with the *ece1Δ/Δ* strain), the number of membrane rupture events is dramatically reduced, though they still occur principally at the JNR and the CCB. This suggests that candidalysin activity acts to 'prime' the invasion pocket towards membrane rupture at the JNR and the CCB. Additionally, candidalysin regulates the formation of the two Gal-3 recruitment patterns strongly correlated to subsequent host cell death ('tubular' and 'elongated'), indicating that its priming activity drives 'destructive' membrane rupture linked to long-term infection damage. Different hypotheses could explain how such a priming mechanism could work: it is possible that low-level damage already present in the 'sub-lytic' invasion pocket is enhanced during JNR or CCB traversal, possibly due to increase in membrane tension, leading to rupture. For example, candidalysin-induced membrane pores (below the threshold of Gal-3 detection) within the 'sub-lytic' invasion pocket may 'stretch' or enlarge during CCB or JNR traversal, resulting in membrane rupture[6]. Alternatively, the 'sub-lytic' invasion pocket may include precursor states of candidalysin assembly prior to complete pore formation, such as those reported by Russell et al.[10], which then mature into fully functional membrane pores during JNR or CCB traversal, leading to membrane rupture. Further research is required to address these and other hypotheses pertaining to the molecular mechanisms underlying candidalysin activity and host damage during *C. albicans* epithelial infection.

As alluded to above, the 'sequential' damage mechanism provides an alternative explanation for the requirement of both hyphal invasion and candidalysin secretion to induce full damage potential during

infection: hyphal extension is required to drive 'sub-lytic' invasion pockets towards the JNR or the CCB, where membrane rupture occurs, a process that cannot be fully replicated by the exogenous addition of candidalysin peptide or by secretion of candidalysin by yeast-locked strains. The 'sequential' damage mechanism may also provide an alternative explanation for the dual innate immune response observed during *C. albicans* epithelial infection, though this remains to be experimentally established (see **Introduction**). This response, proposed to be driven by a concentration-dependent dual-functionality of candidalysin[12], may be attributed instead to the 'sub-lytic' invasion pocket generating the initial pathogen recognition before appreciable damage, followed by traversal of the JNR and CCB resulting in membrane rupture which drives a membrane damage response.

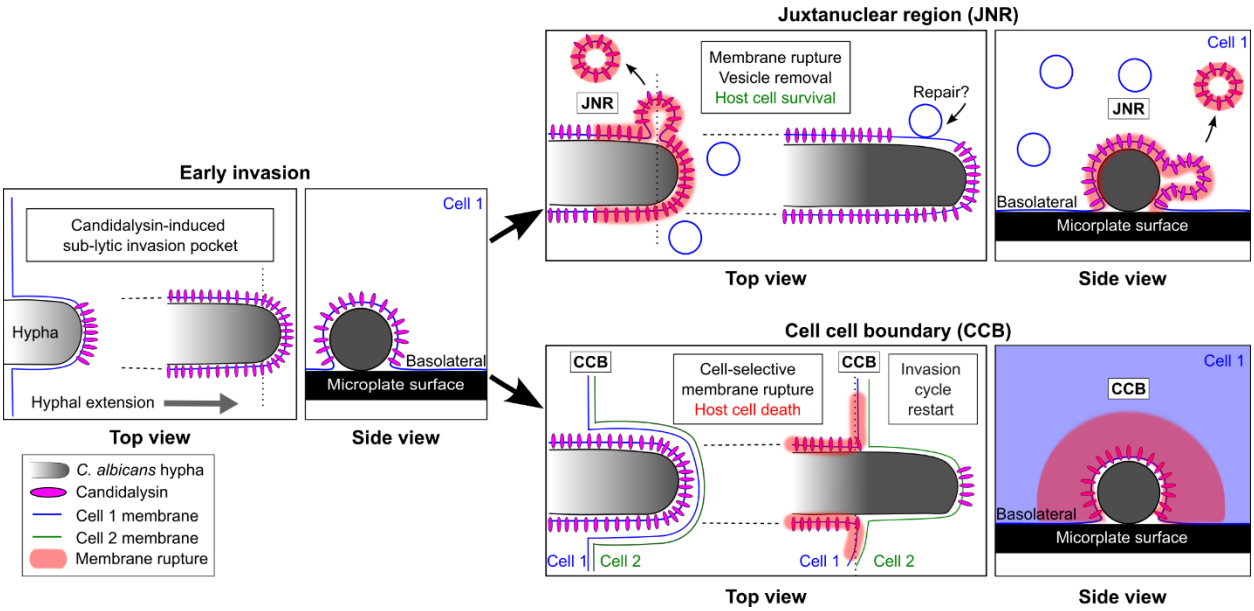

Figure 7. 'Sequential' mechanism for C. albicans epithelial monolayer invasion and damage. *Following an initial apical invasion (see* ***Figure 3****), a hypha extends along the microplate surface invaginating the epithelial basolateral membrane forming a 'partial invasion pocket'. Candidalysin secretion is required for priming a 'sub-lytic' invasion pocket for subsequent membrane rupture. Hyphal extension in proximity to the juxtanuclear region (JNR) results in host membrane rupture followed by removal of vesicles containing ruptured membranes, possibly as part of a regulated host membrane repair response. Hyphal traversal of the cell-cell boundary (CCB) results in cell-selective membrane rupture of the first invaded host cell (Cell 1). The hypha then extends into the second invaded cell (Cell 2), restarting the invasion cycle. Membrane rupture at the CCB is strongly correlated with subsequent host cell death compared to membrane rupture at the JNR, suggesting that CCB traversal is the main driver of long-term infection damage.*

Our work reveals that the CCB is the main site for membrane rupture correlated to subsequent host cell death, suggesting that hyphal traversal of the CCB is the main driver of long-term infection damage in TR146 cells. This result is in line with a previous study of *C. albicans* invasion into non-confluent HeLa cells, which demonstrated that a large portion of membrane rupture events (39%) occurred during hyphal traversal of the cell boundary, primarily resulting in host cell death[5]. In contrast, the same study showed

that CCB traversal during Caco-2 invasion does not lead to membrane rupture or host cell death at early stages of infection, indicating that different epithelial cell types respond differently to CCB traversal, for reasons that are currently not well understood. The CCB includes various junctional complexes (adherens junctions, desmosomes, gap junctions and tight junctions) that anchor transmembrane proteins to the cell cytoskeleton (via actin and intermediate filaments) and to neighboring cells[24]. Thus, the CCB represents a mechanically 'stiff' barrier that appears to counter the extension of hyphae partially enveloped by an invasion pocket, resulting in membrane rupture. CCB traversal by the *ece1Δ/Δ* strain rarely results in membrane rupture and never in host cell death, implying that the 'counter force' exerted by the CCB, which likely leads to increased membrane tension, is sufficient to rupture sub-lytic invasion pocket membranes, but not native (without candidalysin) membranes. We have also observed that CCB rupture is 'cell-selective', damaging only the first invaded cell of the two cells found on each side of the CCB. While the invasion pocket of the first invaded cell at the time of CCB traversal is in a sub-lytic state (having been exposed to candidalysin), membranes of the second invaded cell do not come into direct contact with candidalysin until the invasion pocket of the first cell is ruptured, and are thus 'native' during CCB traversal, likely explaining the cell-selective nature of rupture in this niche. Hyphal extension itself is not blocked by the CCB, a result in line with previous studies demonstrating hyphae can invade substrates with stiffness of between 100-200 kPa compared to the stiffness of epithelia, estimated at 40 - 70 kPa[25]. Of the different junctional complexes, adherens junctions are major determinants of tissue mechanics[26] and were shown to play a key role in *C. albicans* epithelial infection. The *C. albicans* invasins Als3 and Ssa1 have been shown to bind e-cadherin to facilitate induced endocytosis[27,28], while *C. albicans*-secreted aspartic proteinases such as Sap5 can degrade e-cadherin[29]. Indeed, cleavage of c-cadherin has been proposed as one of the mechanisms driving disruption of the intestinal epithelial barrier, resulting in both intracellular and extracellular cleavage events[30]. In addition to adherens junctions, tight junctions also play a role in regulating *C. albicans* invasion of the intestinal barrier [31,32]. Finally, in Caco-2 cells, NFκB activation during infection was shown to stabilize cell-cell junction proteins like E-cadherin, limiting paracellular translocation, while NFκB inhibition allowed hyphae to break down the intercellular barrier in a candidalysin-independent manner[33]. If and how CCB membrane rupture is linked to the various *C. albicans*- cell junction interactions described previously remains to be explored.

Studies in TR146 cells and HeLa cells have shown the presence of a highly regulated host repair response following *C. albicans* induced membrane damage. This response takes multiple forms including Ca^{2+}-dependent autophagic machinery recruitment to the site of damage, ESCRT-dependent membrane blebbing and lysosomal exocytosis[14,34]. More specifically, Westman et al. have shown that during infection of TR146 cells, staining with the lipophilic dye FM4-64 reveals the presence of membrane blebs near the hypha apex which are formed in a candidalysin-dependent manner. As the signal within the blebs was higher than that of the invasion pocket membrane, it was proposed that the observed blebs have undergone membrane rupture. Staining with nanobodies against candidalysin further revealed the presence of candidalysin within the blebs. The authors suggest that Ca^{2+} influx triggered by candidalysin leads to bleb formation, which in turn allows shedding of the toxin along with the blebbing to terminate the Ca^{2+} influx. Additionally, blebs were shown to be associated with the recruitment of ALG-2, ALIX and ESCRT-III, suggested to constrict and extrude the damaged membrane, allowing eventual membrane repair alongside blebbing. Finally, the authors demonstrate the presence of lysosomes at the hyphal apex, and propose that lysosome exocytosis can serve a complementary role in mitigating candidalysin-induced membrane damage, though lysosome recruitment was also observed in cells infected with the *ece1Δ/Δ* mutant. In this study we observe that JNR rupture is often associated with the formation of Gal-3 labelled

vesicles, which are subsequently removed from the site of damage. These observations are consistent with the study by Westman et al., and suggest that JNR rupture and associated vesicle dynamics are part of a regulated host membrane repair response. Indeed, the JNR of TR146 cells was shown to contain lysosomes, further supporting this suggestion[35]. JNR rupture occurs when hyphae enveloped by a basolateral partial invasion pocket extend in proximity to the JNR. This suggests that when close enough, host factors in the JNR can detect sub-lytic invasion pocket membranes leading to rupture. The precise nature of the signaling involved in JNR rupture is not known, though one possibility is that 'sub-lytic' invasion pockets generate a Ca^{2+} influx[14], which in turn is detected by Ca^{2+}-dependent receptors found on JNR-associated vesicles. Overall, the specific features associated with JNR rupture (vesicle formation and removal), the weak correlation of JNR rupture with host cell death compared to CCB rupture, and the 'non-destructive' 'tip' Gal-3 recruitment pattern associated with this niche, all point towards JNR rupture acting as part of a regulated host membrane repair response, whose precise nature remains to be determined.

In conclusion, in this work we propose a new mechanism underlying host damage during *C. albicans* epithelial infection, based on candidalysin priming of subsequent host membrane rupture occurring at distinct subcellular niches. As the results reported in this study are based on a highly simplified *in vitro* monolayer infection model using an immortalized epithelial cell line, their relevance to more complex infection models, and most importantly, to real-life *C. albicans* epithelial infection remains to be determined. Future research employing advanced *in vitro* as well as *in vivo* infection models, should enable addressing the limitations imposed by the experimental model used here, while also testing the novel hypotheses and mechanisms arising from this study.

Materials and methods

Candida albicans strains and growth conditions

Candida albicans BWP17+CIp30 (prototroph wildtype) (genotype rps1::(HIS1 ARG4 URA3) URA3::imm434/URA3::imm434 IRO1::imm434/IRO1::imm434 HIS1::hisG/HIS1::hisG chr5Part::Δ ARG4::hisG/ARG4::hisG RPS1::(HIS1 ARG4 URA3)) or ece1ha+CIp10 ece1 double knockout mutant (Genotype ece1::HIS1/ece1::ARG4 rps1::URA3 URA3::imm434/URA3::imm434 IRO1::imm434/IRO1::imm434 HIS1::hisG/HIS1::hisG chr5Part::Δ ARG4::hisG/ARG4::hisG ECE1::HIS1/ECE1::ARG4 RPS1::URA3)[6], kindly provided by Bernhard Hube (Leibniz Institute for Natural Product Research and Infection Biology-Hans Knoell Institute , Jena, Germany) were used as indicated. Strains were routinely grown on Yeast Extract Peptone Dextrose (YEPD) liquid/agar (1% yeast extract, 2% peptone, 2% D-glucose with or without 2% agar) supplemented with 80 µg/mL of uridine at 30°C.

Epithelial cell lines culture

TR146 cell line expressing mOrange-Galectin-3 (Gal-3) was generated by Patricia Latour Lambert (Pasteur Institute, Paris, France) using the Sleeping Beauty plasmid (pSBBi-PUR[36]) with the coding sequences from the pEmOrangeGalectin3. Cells were routinely cultured in Dulbecco's modified Eagle's medium (DMEM) high glucose (Gibco-Invitrogen) supplemented with 10% fetal bovine calf serum (Gibco-Invitrogen) and 1% penicillin-streptomycin ((10,000 U/mL) Gibco) at 37°C, 5% CO2. Live-cell imaging was performed in optically transparent EM medium (120 mM NaCl, 7 mM KCl, 1.8 mM CaCl2, 0.8 mM MgCl2, 5 mM glucose

and 25 mM Hepes at pH 7.3) supplemented with 0.2 g/L of amino acids (MP Biomedicals SC Amino Acids Mix) and 80 µg/mL of uridine[5].

Infection procedure

For all experiments, TR146 cells were plated in a µ-Plate 96 Well Black (Ibidi, Cat. 89626). $3x10^5$ cells/mL were plated 2 days before infection and were infected at 100% confluency. To label the host cell plasma membrane and endocytic compartment, CellMask Deep Red Plasma Membrane Stain (CM) (ThermoFisher) was used at a concentration of 2.5 µg/mL in EM media. TR146 cells were incubated with CM in the dark at 37°C for 10 minutes and then washed once with PBS (Gibco). SYTOX Green Nucleic Acid Stain (Invitrogen) was used as a cell death marker at a concentration of 100 nM in EM media throughout infection.

For infection, *C. albicans* strains were cultured overnight in liquid YEPD supplemented with 80 µg/mL uridine at 30°C, 200 rpm shaking, followed by a 1:100 back dilution into fresh YEPD and grown to exponential phase at 30°C, 200 rpm shaking for 4 hours. To prevent yeast from forming large clumps, the culture was subjected to mild sonication on ice for 6 cycles of 15 seconds on and 30 seconds off, at power setting 15% using a FisherBrand Model 50 Sonic Dismembrator (Fisher Scientific) with a standard ⅛" diameter microtip. Sonicated yeast cells were counted with a LUNA-FL reader (Logos Biosystems) and then diluted in EM medium and added to epithelial cells at a multiplicity of infection (MOI) 0.001 ($1x10^3$ yeast cells/mL, 100 µL in each well). 30 min of 'landing time' to allow initial adherence of yeast to epithelial cells was followed by inoculating yeast (IY) identification and alignment and live cell imaging.

Live-cell imaging

Live cell imaging was performed in a fully automated Inverted Nikon Ti2 Crest V3 spinning disk confocal equipped with Perfect focus system (PFS) and environmental chamber set to 37°C and 5% CO_2. For 24 hours acquisitions a 20x objective (NA 0.8) was used, with acquisition intervals of 30 min. For 12 hour acquisitions a 40X water objective (NA 1.15) linked to a water dispenser (Nikon) was used, with acquisition intervals of 10 min. Z stack of 12 planes, 1 µm step was used, with 8 FOVs acquired per condition (WT, *ece1Δ/Δ*) plus 4 FOVs for non-infected controls in 24-hour acquisitions. For the Bright-field (BF) channel, only a single central z-section was acquired. For "high-resolution" 2-hour acquisitions, a 60X oil immersion objective (NA 1.42) was used, with acquisition intervals of 2 min. Z stack of 13 planes, 0.5 µm step was used, with 6 FOVs acquired of WT infection. 20X acquisitions were used for analysis in Figure 2B. 40X acquisitions are presented and used for analysis in Figures 1, 2A, 3A, 4, 5B, 5C, 5D. 60X acquisitions are presented and used for analysis in Figure 3C, 5A, 6.

Image processing and analysis

Data was analyzed using NIS-Elements (Nikon), Fiji[37] and CellProfiler[38]. Galectin-3 recruitment sites were identified and annotated manually. Host cell death as indicated by SYTOX Green was quantified using CellProfiler. Figures were prepared using NIS-Elements, Fiji and Inkscape.

Quantifications, statistical analysis and reproducibility

24 hours live cell imaging data were acquired in three independent experiments. 12 hours live cell imaging data was acquired in four independent experiments. For all quantifications of Gal-3 recruitment, the first 600 minutes of each acquisition were analysed. 2 hours live cell imaging data was acquired in two

independent experiments. Data was analysed using RStudio. p-value thresholds: 0.05 (*), 0.01 (**), 0.001 (***). ANOVA test and student t-test were performed in Figure 2B, 2C, 2E (ANOVA only), 2F. $\chi 2$ test for homogeneity was performed in Figure 4B, 5B, 5C, and 5D. Student t-test was performed in Figure 4C, error bars represent SEM.

Data availability

Live cell imaging datasets from this study are available from the corresponding author upon request due to data size and multi-parametric format.

References

1. Gow, N. A. R., van de Veerdonk, F. L., Brown, A. J. P. & Netea, M. G. Candida albicans morphogenesis and host defence: discriminating invasion from colonization. *Nat Rev Microbiol* (2011) doi:10.1038/nrmicro2711.
2. Brown, G. D. *et al.* Hidden killers: human fungal infections. *Sci Transl Med* **4**, (2012).
3. Höfs, S., Mogavero, S. & Hube, B. Interaction of Candida albicans with host cells: virulence factors, host defense, escape strategies, and the microbiota. *Journal of Microbiology* vol. 54 149–169 Preprint at https://doi.org/10.1007/s12275-016-5514-0 (2016).
4. Dalle, F. *et al.* Cellular interactions of Candida albicans with human oral epithelial cells and enterocytes. *Cell Microbiol* **12**, 248–271 (2010).
5. Lachat, J. *et al.* Trans-cellular tunnels induced by the fungal pathogen Candida albicans facilitate invasion through successive epithelial cells without host damage. *Nat Commun* **13**, 3781 (2022).
6. Moyes, D. L. *et al.* Candidalysin is a fungal peptide toxin critical for mucosal infection. *Nature* **532**, 64–68 (2016).
7. Mogavero, S. *et al.* Candidalysin delivery to the invasion pocket is critical for host epithelial damage induced by Candida albicans. *Cell Microbiol* **23**, (2021).
8. Wilson, D., Naglik, J. R. & Hube, B. The Missing Link between Candida albicans Hyphal Morphogenesis and Host Cell Damage. *PLoS Pathogens* vol. 12 e1005867 Preprint at https://doi.org/10.1371/journal.ppat.1005867 (2016).
9. Lin, J. *et al.* Sulfated glycosaminoglycans are host epithelial cell targets of the Candida albicans toxin candidalysin. *Nature Microbiology 2024 9:10* **9**, 2553–2569 (2024).
10. Russell, C. M. *et al.* The Candida albicans virulence factor candidalysin polymerizes in solution to form membrane pores and damage epithelial cells. *Elife* **11**, (2022).
11. Allert, S. *et al.* Candida albicans-induced epithelial damage mediates translocation through intestinal barriers. *mBio* **9**, (2018).
12. Richardson, J. P., Moyes, D. L., Ho, J. & Naglik, J. R. Candida innate immunity at the mucosa. *Semin Cell Dev Biol* (2018) doi:10.1016/j.semcdb.2018.02.026.
13. Wächtler, B. *et al.* Candida albicans-epithelial interactions: dissecting the roles of active penetration, induced endocytosis and host factors on the infection process. *PLoS One* **7**, e36952 (2012).

14. Westman, J. *et al.* Calcium-dependent ESCRT recruitment and lysosome exocytosis maintain epithelial integrity during Candida albicans invasion. *Cell Rep* **38**, (2022).

15. Almeida, R. S. *et al.* the hyphal-associated adhesin and invasin Als3 of Candida albicans mediates iron acquisition from host ferritin. *PLoS Pathog* **4**, e1000217 (2008).

16. Paz, I. *et al.* Galectin-3, a marker for vacuole lysis by invasive pathogens. *Cell Microbiol* **12**, 530–544 (2010).

17. Weiner, A. *et al.* Macropinosomes are Key Players in Early Shigella Invasion and Vacuolar Escape in Epithelial Cells. *PLoS Pathog* **12**, e1005602 (2016).

18. Ellison, C. J., Kukulski, W., Boyle, K. B., Munro, S. & Randow, F. Transbilayer Movement of Sphingomyelin Precedes Catastrophic Breakage of Enterobacteria-Containing Vacuoles. *Current Biology* **30**, 2974-2983.e6 (2020).

19. Gutierrez, M. G. & Enninga, J. Intracellular niche switching as host subversion strategy of bacterial pathogens. *Current Opinion in Cell Biology* vol. 76 Preprint at https://doi.org/10.1016/j.ceb.2022.102081 (2022).

20. Richardson, J. P. *et al.* Candidalysin Drives Epithelial Signaling, Neutrophil Recruitment, and Immunopathology at the Vaginal Mucosa. *Infect Immun* **86**, (2018).

21. Swidergall, M. *et al.* Candidalysin Is Required for Neutrophil Recruitment and Virulence During Systemic Candida albicans Infection. *J Infect Dis* **220**, 1477 (2019).

22. Schaller, M., Zakikhany, K., Naglik, J. R., Weindl, G. & Hube, B. Models of oral and vaginal candidiasis based on in vitro reconstituted human epithelia. *Nat Protoc* **1**, 2767–73 (2006).

23. Russell, C. M., Rybak, J. A., Miao, J., Peters, B. M. & Barrera, F. N. Candidalysin: Connecting the pore forming mechanism of this virulence factor to its immunostimulatory properties. *J Biol Chem* **299**, (2023).

24. Fu, R., Jiang, X., Li, G., Zhu, Y. & Zhang, H. Junctional complexes in epithelial cells: sentinels for extracellular insults and intracellular homeostasis. *FEBS J* **289**, 7314–7333 (2022).

25. Puerner, C. *et al.* Mechanical force-induced morphology changes in a human fungal pathogen. *BMC Biol* **18**, (2020).

26. Lenne, P. F., Rupprecht, J. F. & Viasnoff, V. Cell Junction Mechanics beyond the Bounds of Adhesion and Tension. *Dev Cell* **56**, 202–212 (2021).

27. Phan, Q. T. *et al.* Als3 is a Candida albicans invasin that binds to cadherins and induces endocytosis by host cells. *PLoS Biol* **5**, e64 (2007).

28. Sun, J. N. *et al.* Host Cell Invasion and Virulence Mediated by Candida albicans Ssa1. *PLoS Pathog* **6**, e1001181 (2010).

29. Villar, C. C., Kashleva, H., Nobile, C. J., Mitchell, A. P. & Dongari-Bagtzoglou, A. Mucosal tissue invasion by Candida albicans is associated with E-cadherin degradation, mediated by transcription factor Rim101p and protease Sap5p. *Infect Immun* **75**, 2126–2135 (2007).

30. Frank, C. F. & Hostetter, M. K. Cleavage of E-cadherin: a mechanism for disruption of the intestinal epithelial barrier by Candida albicans. *Transl Res* **149**, 211–222 (2007).

31. Goyer, M. *et al.* Intestinal Cell Tight Junctions Limit Invasion of Candida albicans through Active Penetration and Endocytosis in the Early Stages of the Interaction of the Fungus with the Intestinal Barrier. *PLoS One* **11**, e0149159 (2016).

32. Böhringer, M. *et al.* Candida albicans infection leads to barrier breakdown and a MAPK/NF-κB mediated stress response in the intestinal epithelial cell line C2BBe1. *Cell Microbiol* **18**, 889–904 (2016).

33. Sprague, J. L. *et al.* Candida albicans translocation through the intestinal epithelial barrier is promoted by fungal zinc acquisition and limited by NFκB-mediated barrier protection. *PLoS Pathog* **20**, (2024).

34. Lapaquette, P. *et al.* Membrane protective role of autophagic machinery during infection of epithelial cells by *Candida albicans*. *Gut Microbes* **14**, (2022).

35. Wayakanon, K. *et al.* Polymersome-mediated intracellular delivery of antibiotics to treat Porphyromonas gingivalis-infected oral epithelial cells. *FASEB J* **27**, 4455–4465 (2013).

36. Kowarz, E., Löscher, D. & Marschalek, R. Optimized Sleeping Beauty transposons rapidly generate stable transgenic cell lines. *Biotechnol J* **10**, 647–653 (2015).

37. Schindelin, J. *et al.* Fiji: An open-source platform for biological-image analysis. *Nature Methods* vol. 9 676–682 Preprint at https://doi.org/10.1038/nmeth.2019 (2012).

38. Stirling, D. R. *et al.* CellProfiler 4: improvements in speed, utility and usability. *BMC Bioinformatics* **22**, (2021).

Acknowledgements

We thank Bernhard Hube (Leibniz Institute for Natural Product Research and Infection Biology-Hans Knoell Institute, Jena, Germany) for providing us with the *C. albicans* strains used in this study. We thank Jost Enninga (Pasteur Institute, Paris, France), for support in production of stably expressing epithelial cell lines. We thank Robert Arkowitz (IBV, Université Côte d'Azur, Nice France) for critical reading of the manuscript. We thank UMS28 in Sorbonne University for support with BSL2 facility and microscopy. This work was supported by the ATIP-Avenir program to AW and by the Conseil Régional d'Île-de-France via the DIM1Health action for funding of the spinning disk confocal microscope.

Contributions

Conceptualization, A.W.; Methodology, N.C., L.M., A.S, P.L, J.F., M.L and A.W.; Investigation, N.C., L.M., A.S. and A.W.; Formal Analysis, N.C., L.M., A.S. M.L and A.W; Writing - Original Draft, A.W.; Supervision, A.W.

Competing interests

The authors declare no competing interests

A Experimental procedure

mOrange-Gal-3-TR146 seeding
(96-well microplate format)

Staining epithelial cells with
SYTOX Green + CellMask Deep Red

Infection with *C. albicans* BWP17 (WT) or ece1Δ/Δ
MOI 0.001

Identification of inoculating yeast (IY)

Live cell imaging
12 hours (10 min interval) or 24 hours (30 min interval)
depending on experiment

B Inoculating yeast identification

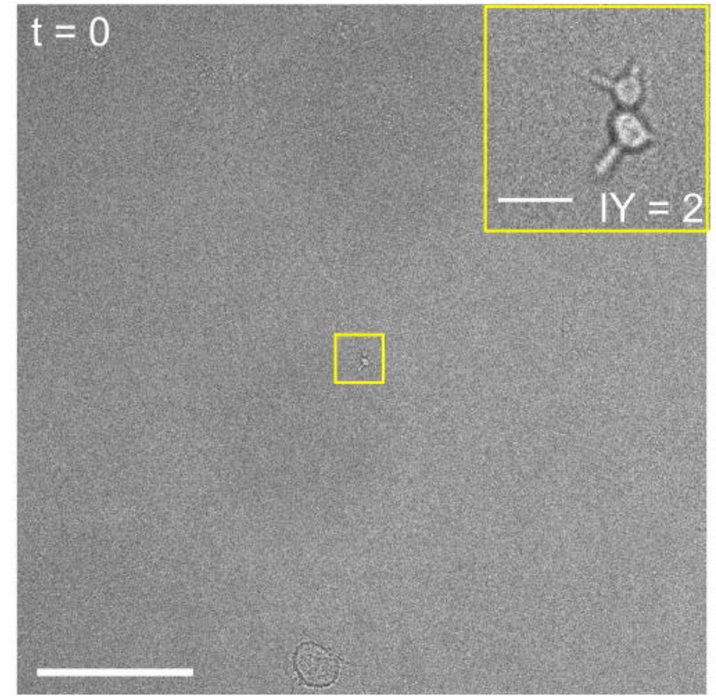

Time: 0 (acquistion launch)

Inoculating yeast (IY) number = 2

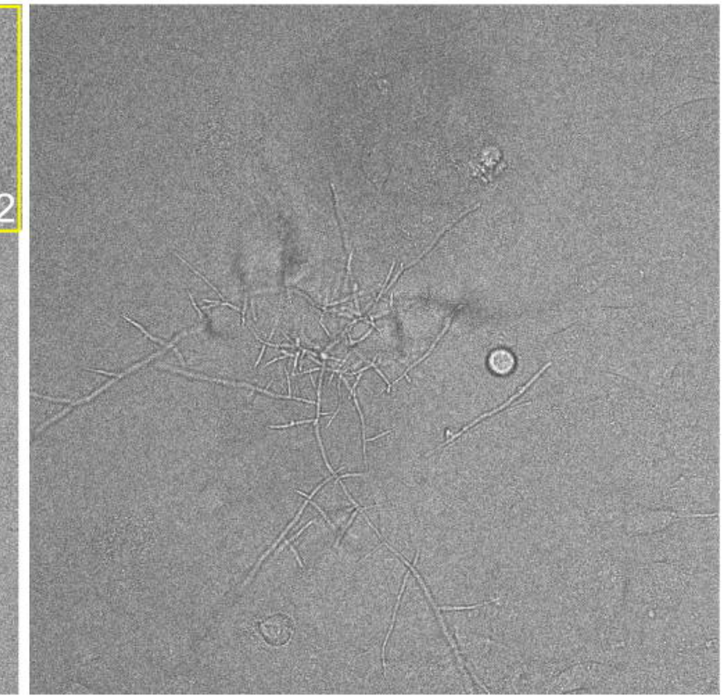

Time: 600 min

All hyphae within field-of-view (FOV) derived from IY identified at time 0

C Live cell imaging

BF | SYTOX Green | mOrange-Gal-3 | CellMask

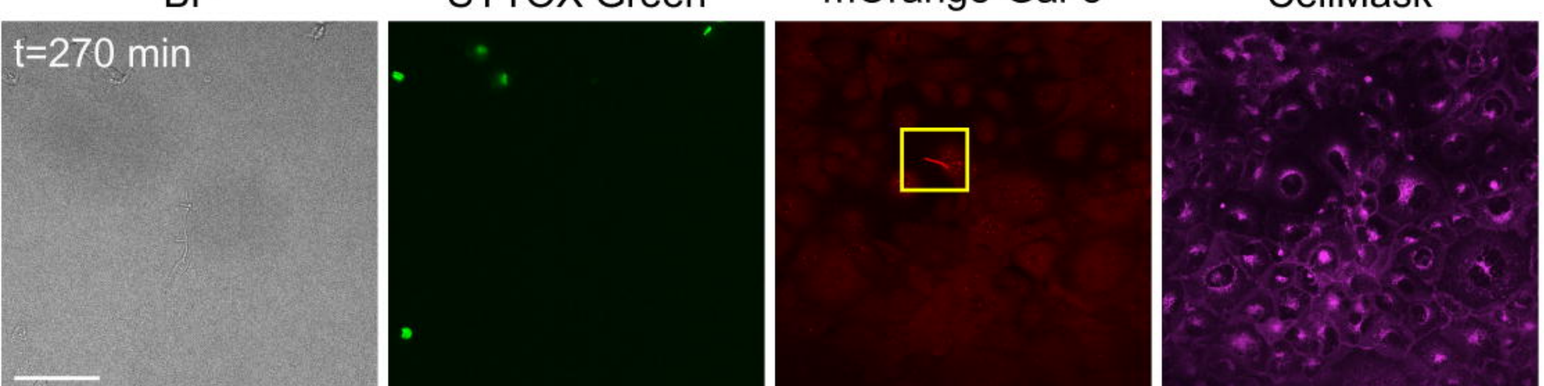

Inset

mOrange-Gal-3 | CellMask | mOrange-Gal-3 CellMask

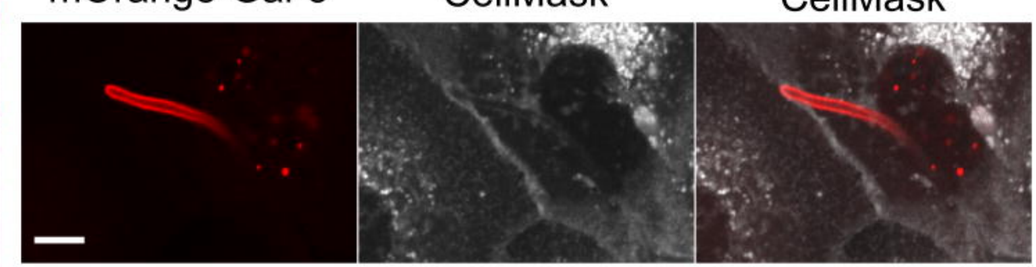

Galectin-3 recruitment event

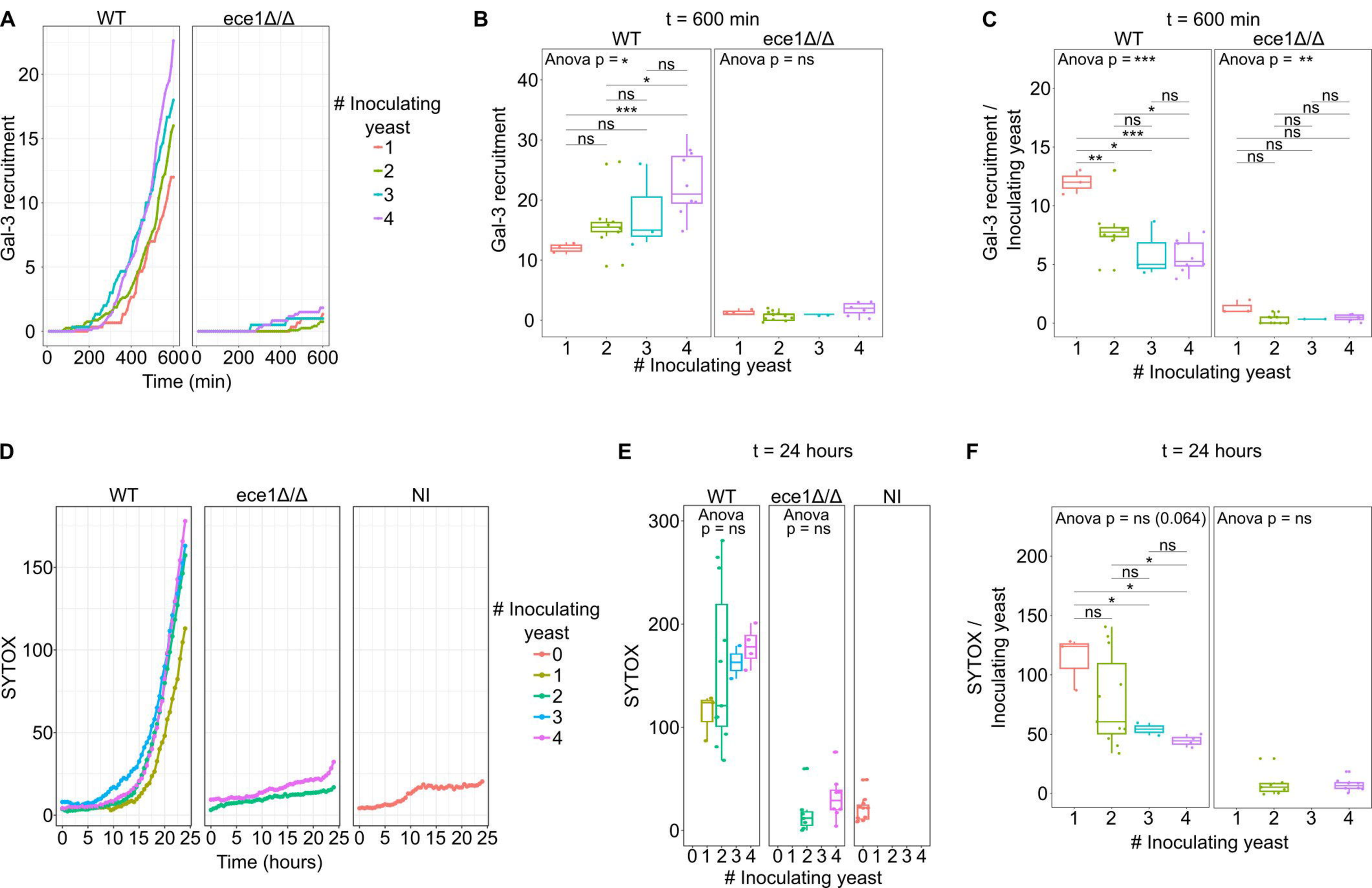
A
WT
ece1Δ/Δ
Gal-3 recruitment
Time (min)
Inoculating yeast
1
2
3
4
B
t = 600 min
WT
ece1Δ/Δ
Anova p = *
Anova p = ns
Gal-3 recruitment
Inoculating yeast
C
t = 600 min
WT
ece1Δ/Δ
Anova p = ***
Anova p = **
Gal-3 recruitment / Inoculating yeast
Inoculating yeast
D
WT
ece1Δ/Δ
NI
SYTOX
Time (hours)
Inoculating yeast
0
1
2
3
4
E
t = 24 hours
WT
ece1Δ/Δ
NI
Anova p = ns
Anova p = ns
SYTOX
Inoculating yeast
F
t = 24 hours
Anova p = ns (0.064)
Anova p = ns
SYTOX / Inoculating yeast
Inoculating yeast

A

Overview

Gal-3 CM

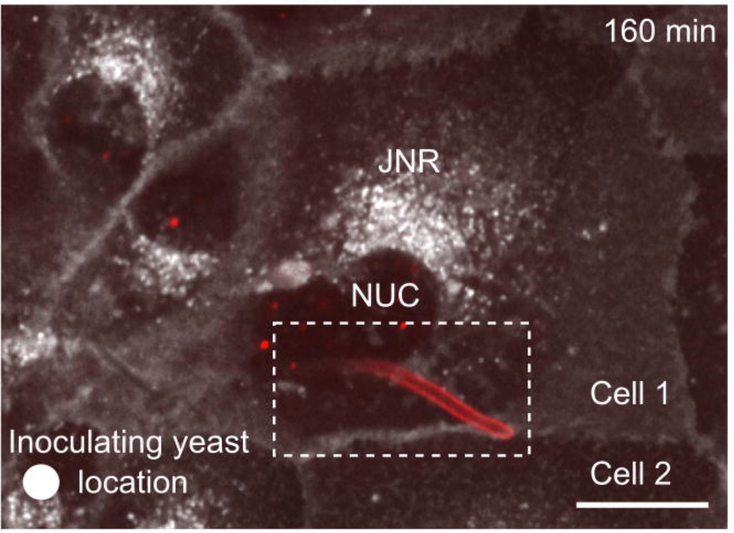

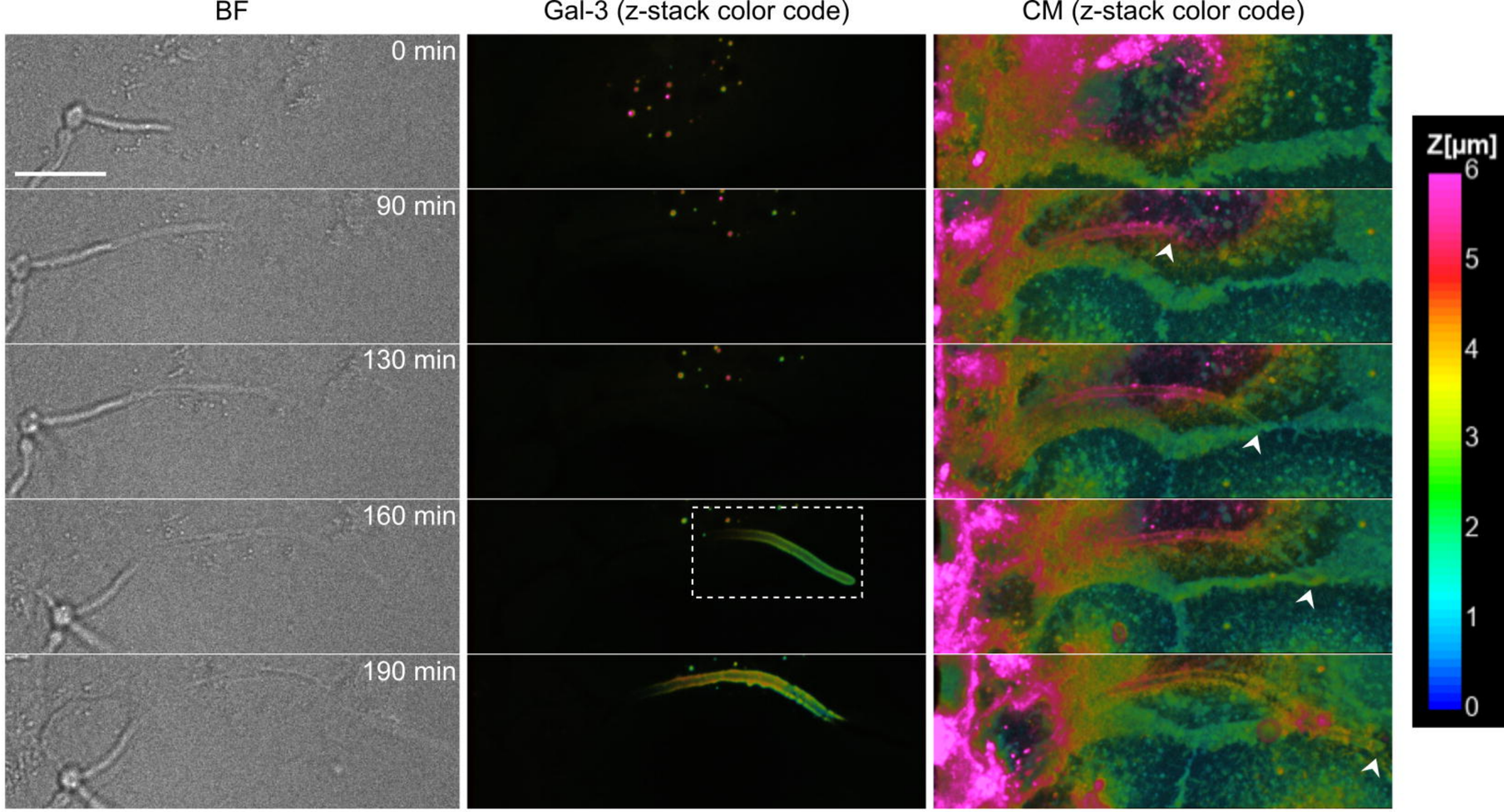

B

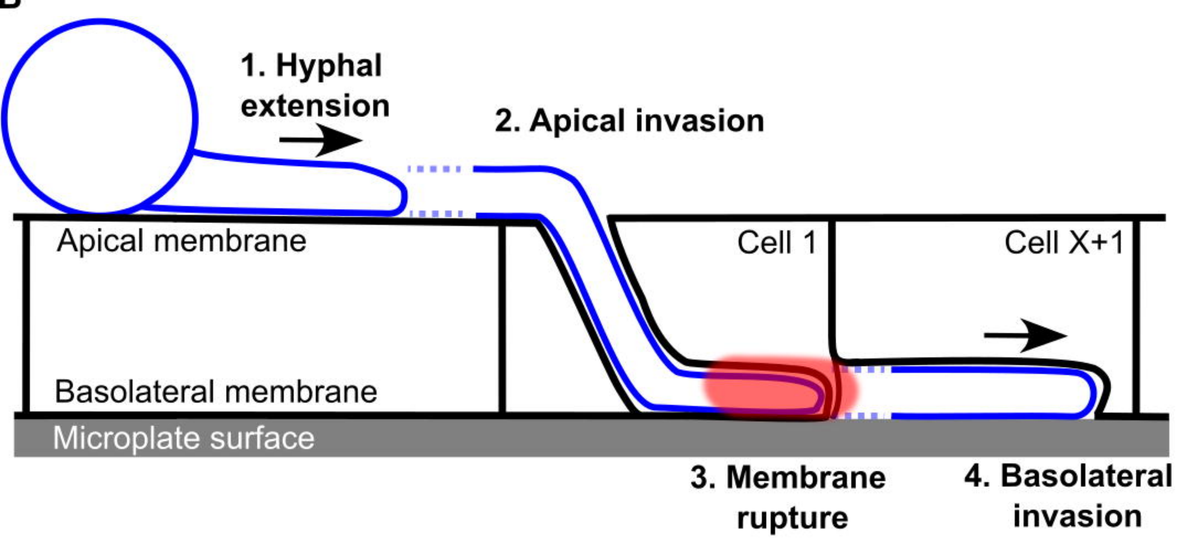

C

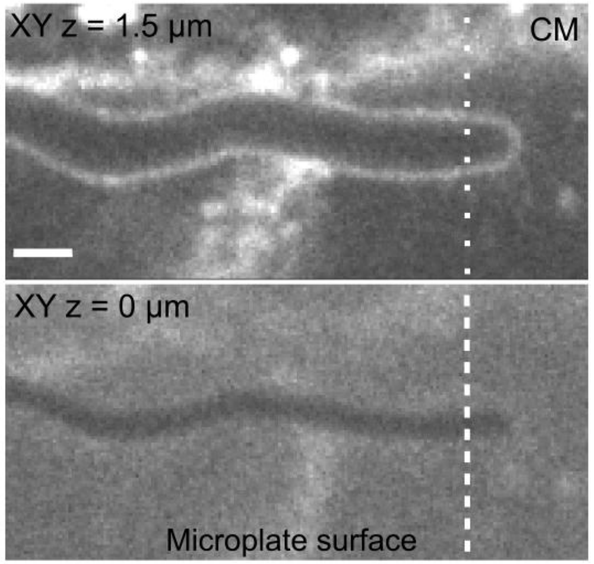

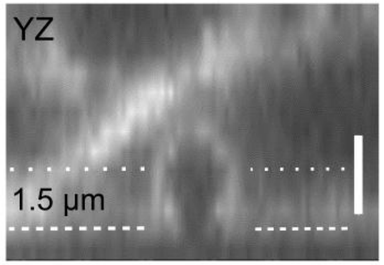

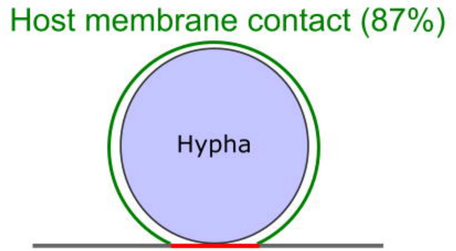

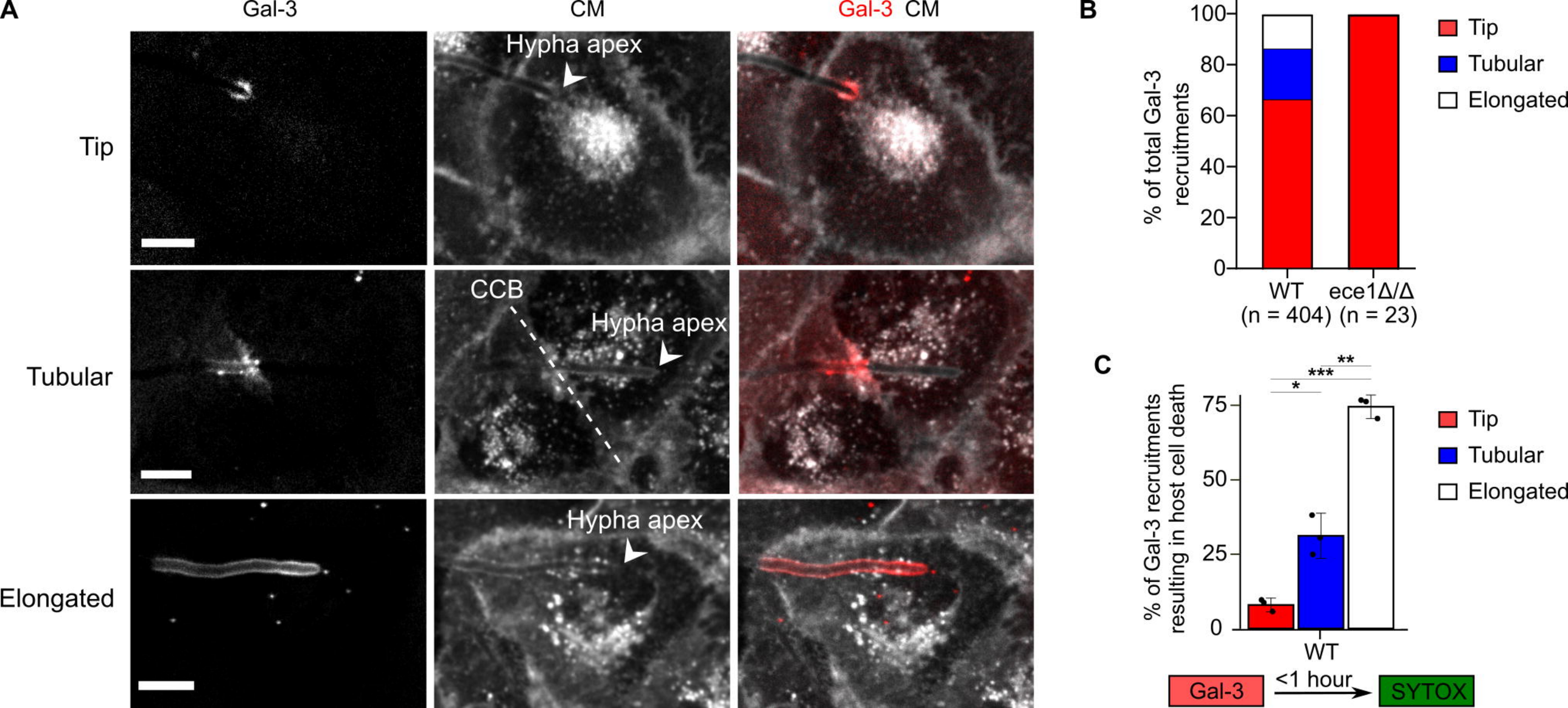
A
Gal-3
CM
Gal-3 CM
Tip
Tubular
Elongated
Hypha apex
CCB
Hypha apex
Hypha apex
B
% of total Gal-3 recruitments
100
80
60
40
20
0
WT
(n = 404)
ece1Δ/Δ
(n = 23)
Tip
Tubular
Elongated
C
% of Gal-3 recruitments resulting in host cell death
75
50
25
0
*
***
**
WT
Tip
Tubular
Elongated
Gal-3
<1 hour
SYTOX

A

Overview of the path of invasion

Gal-3 CM

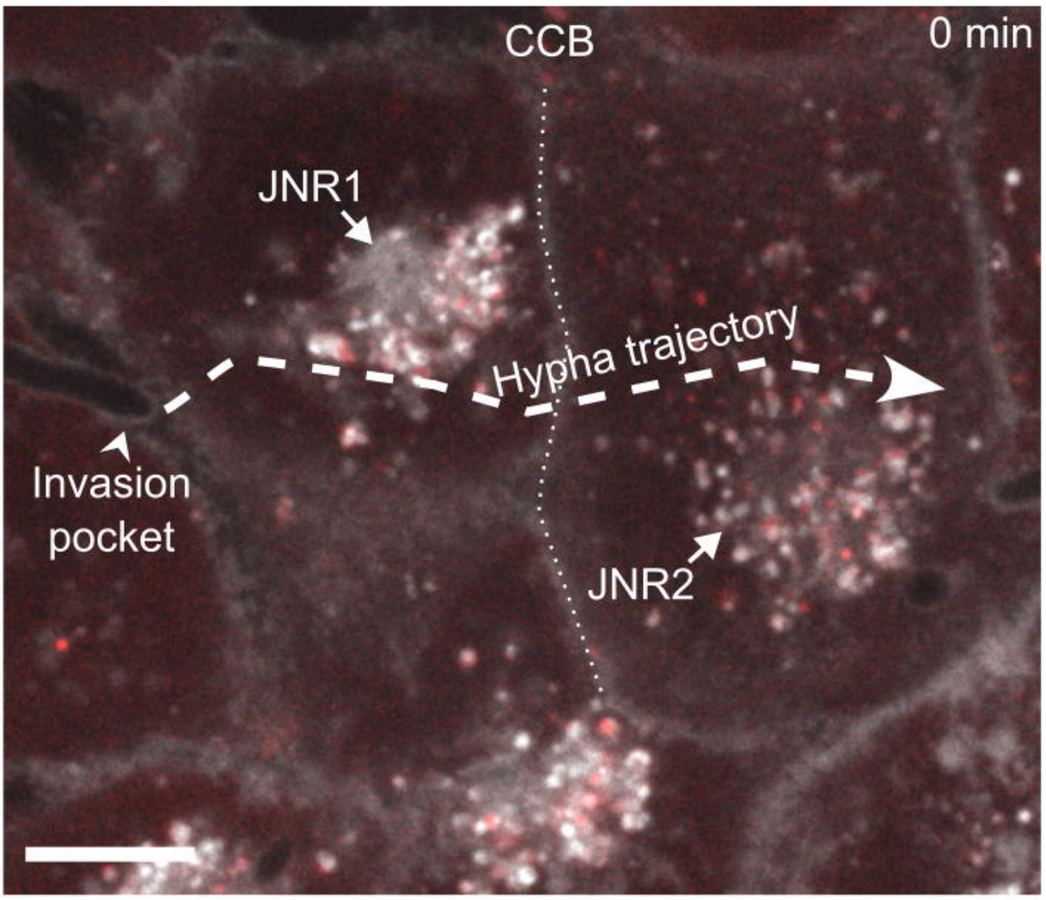

JNR: Juxtanuclear region
CCB: Cell-cell boundary

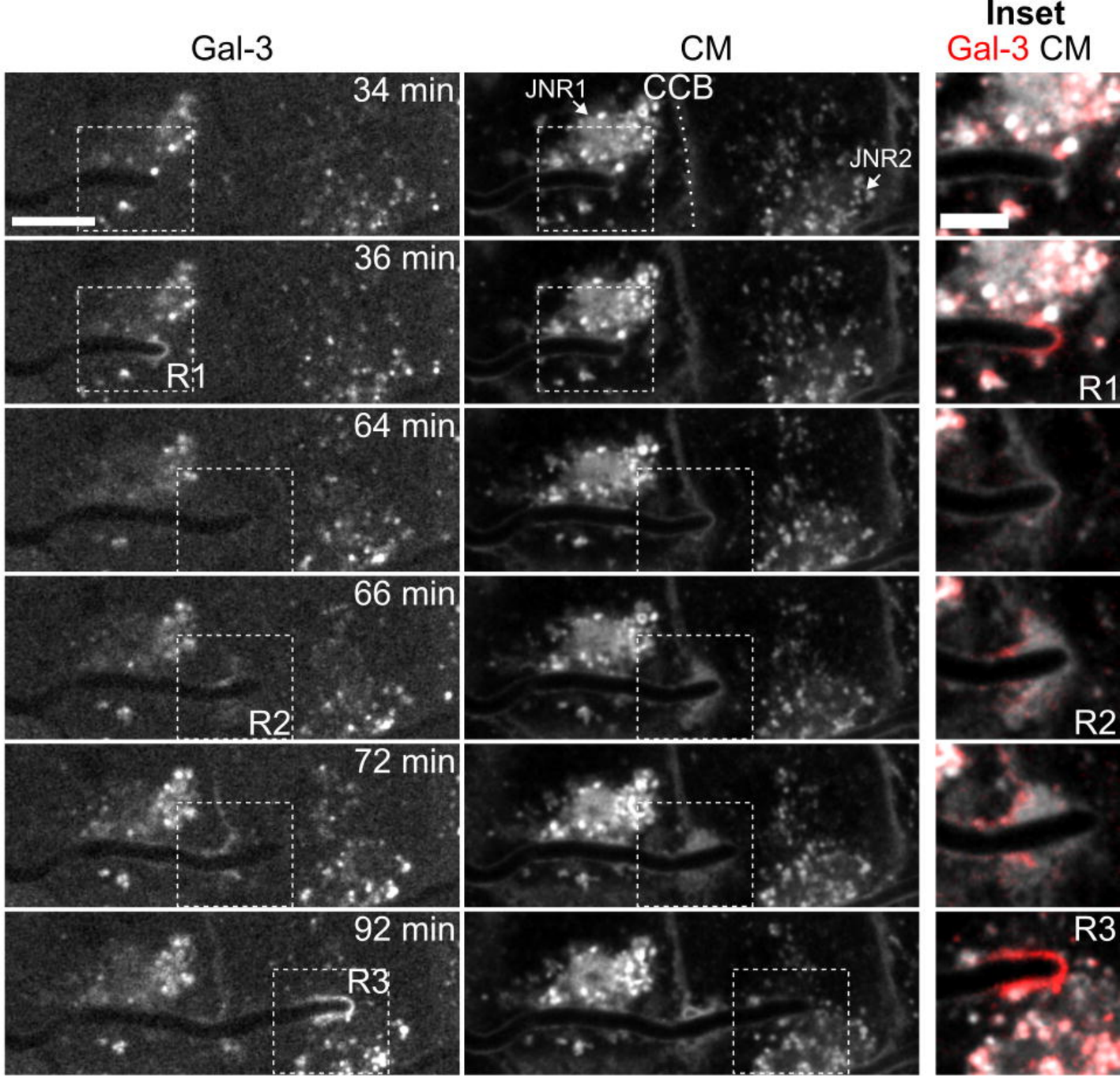

B

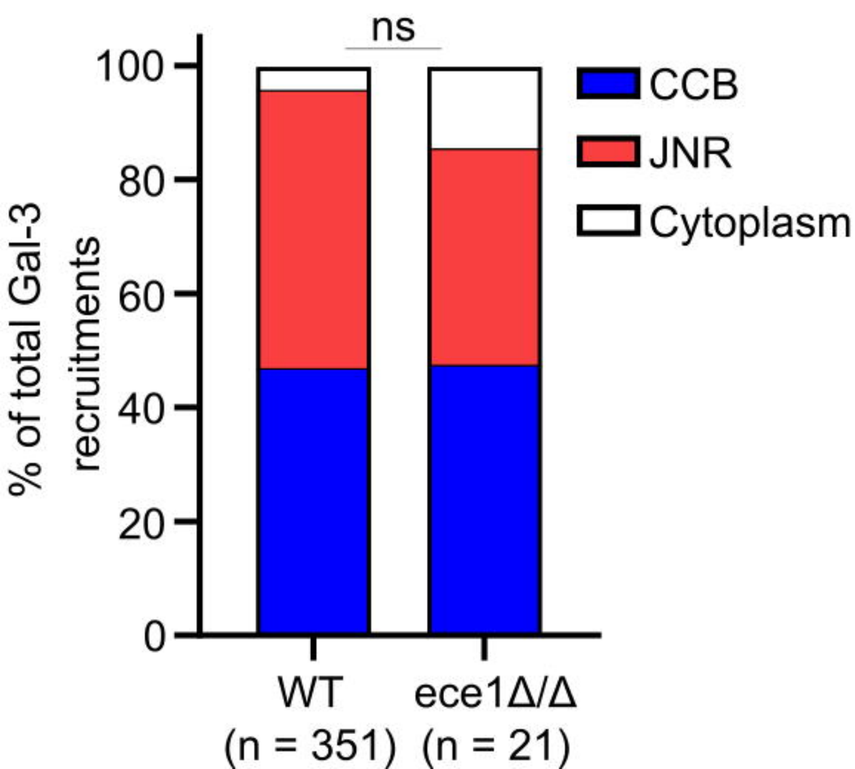

C

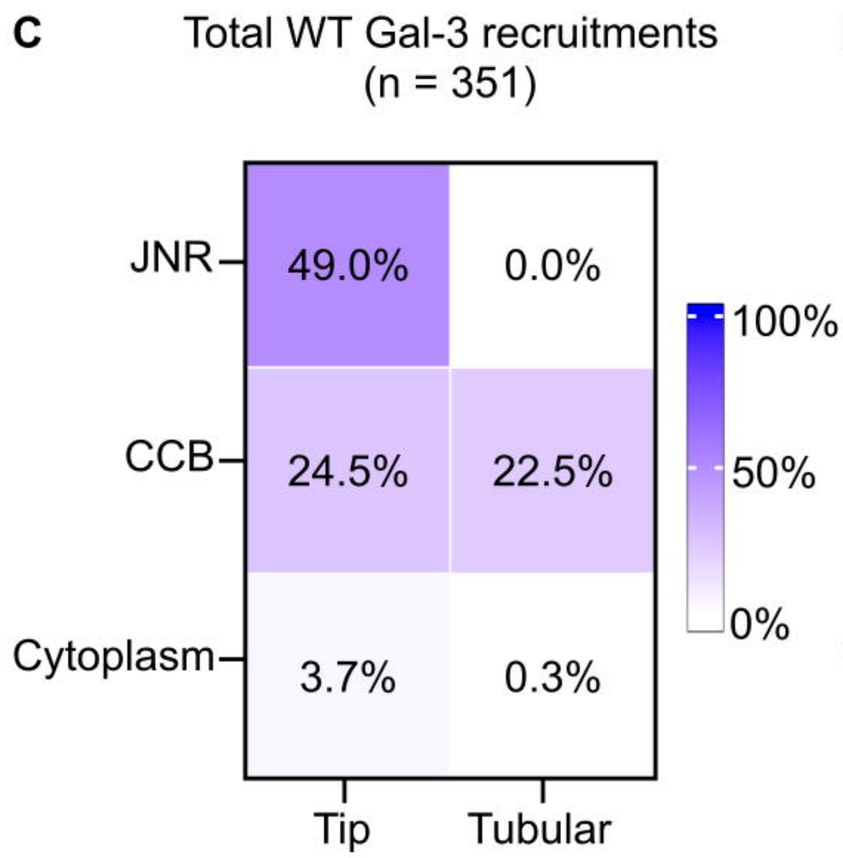

D

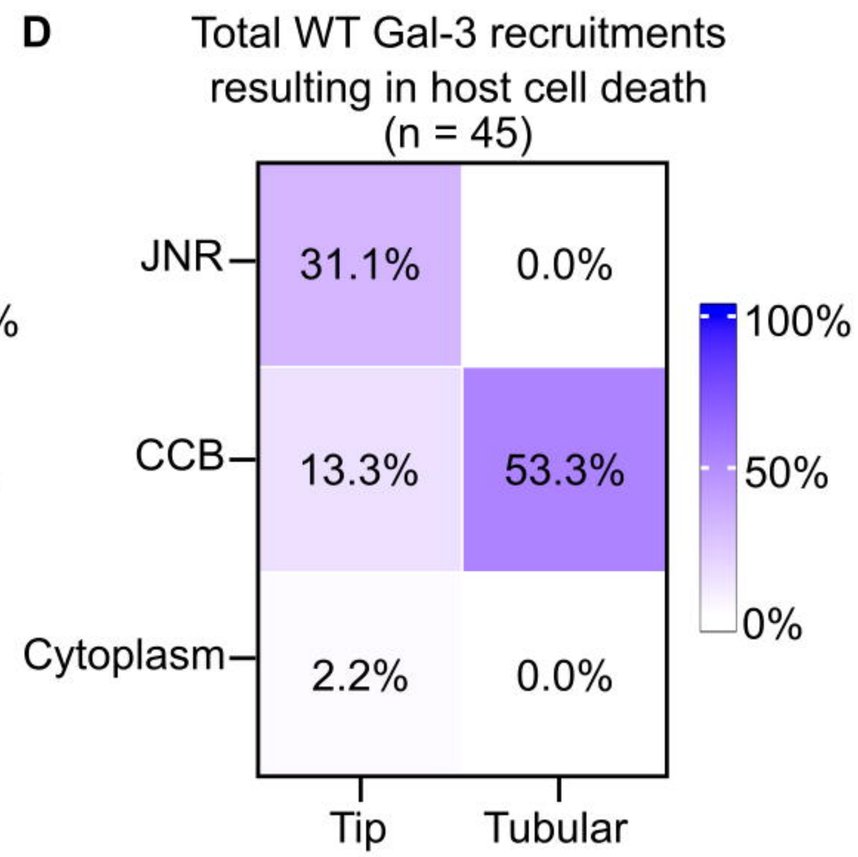

A Cell-cell boundary (CCB)

Overview

Gal-3 CM

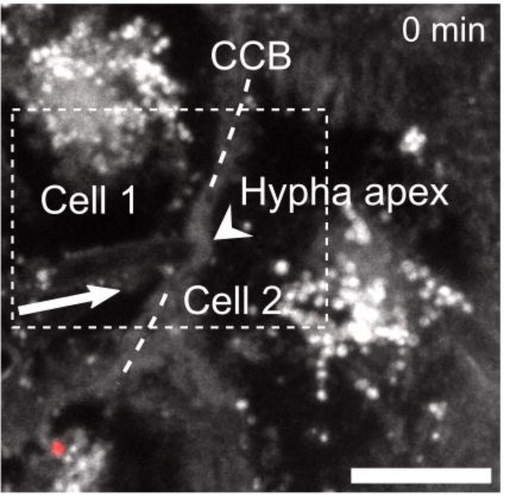

Inset

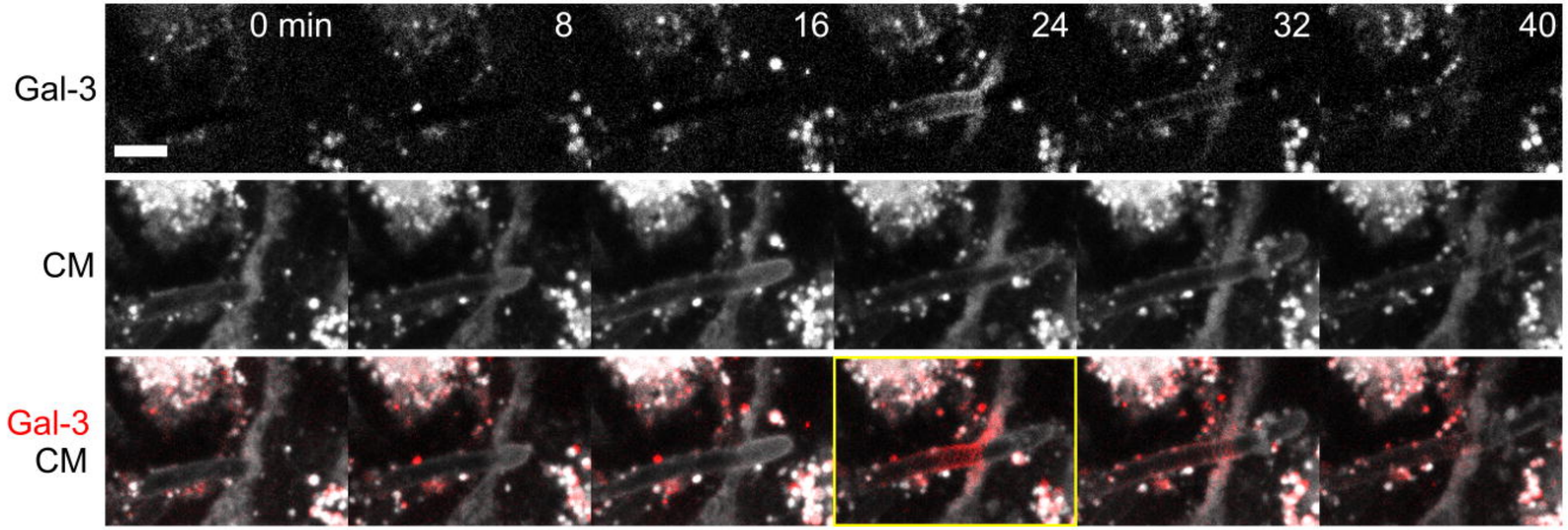

Key frame

Gal-3 CM

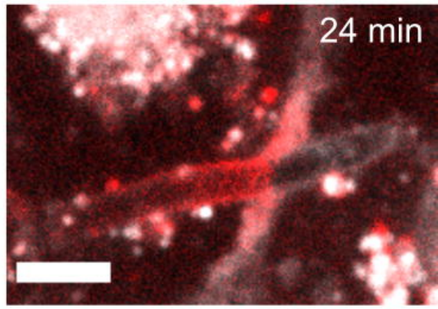

B Juxtanuclear region (JNR)

Overview

Gal-3 CM

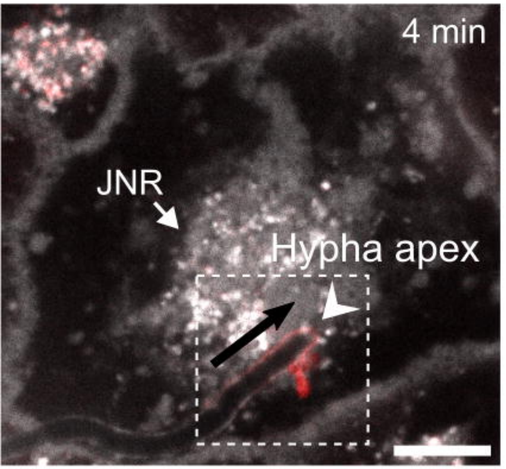

Inset

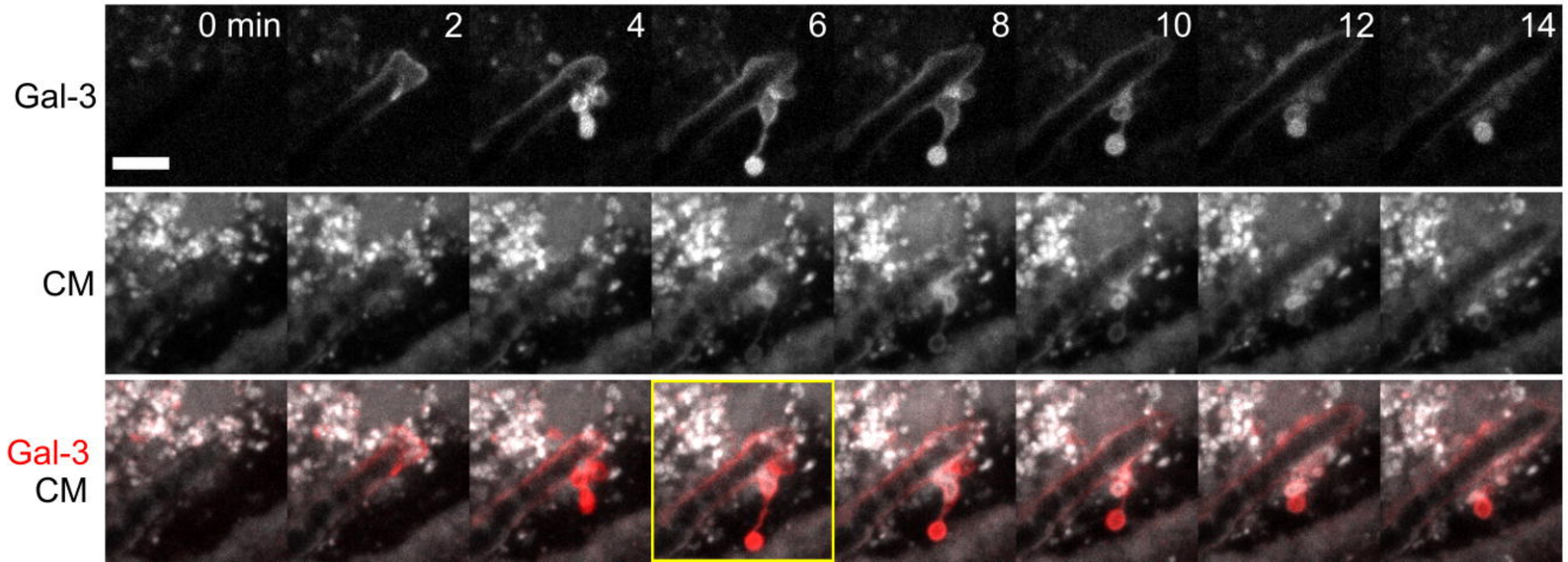

Key frame

Gal-3 CM

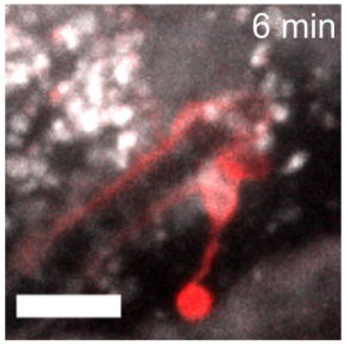

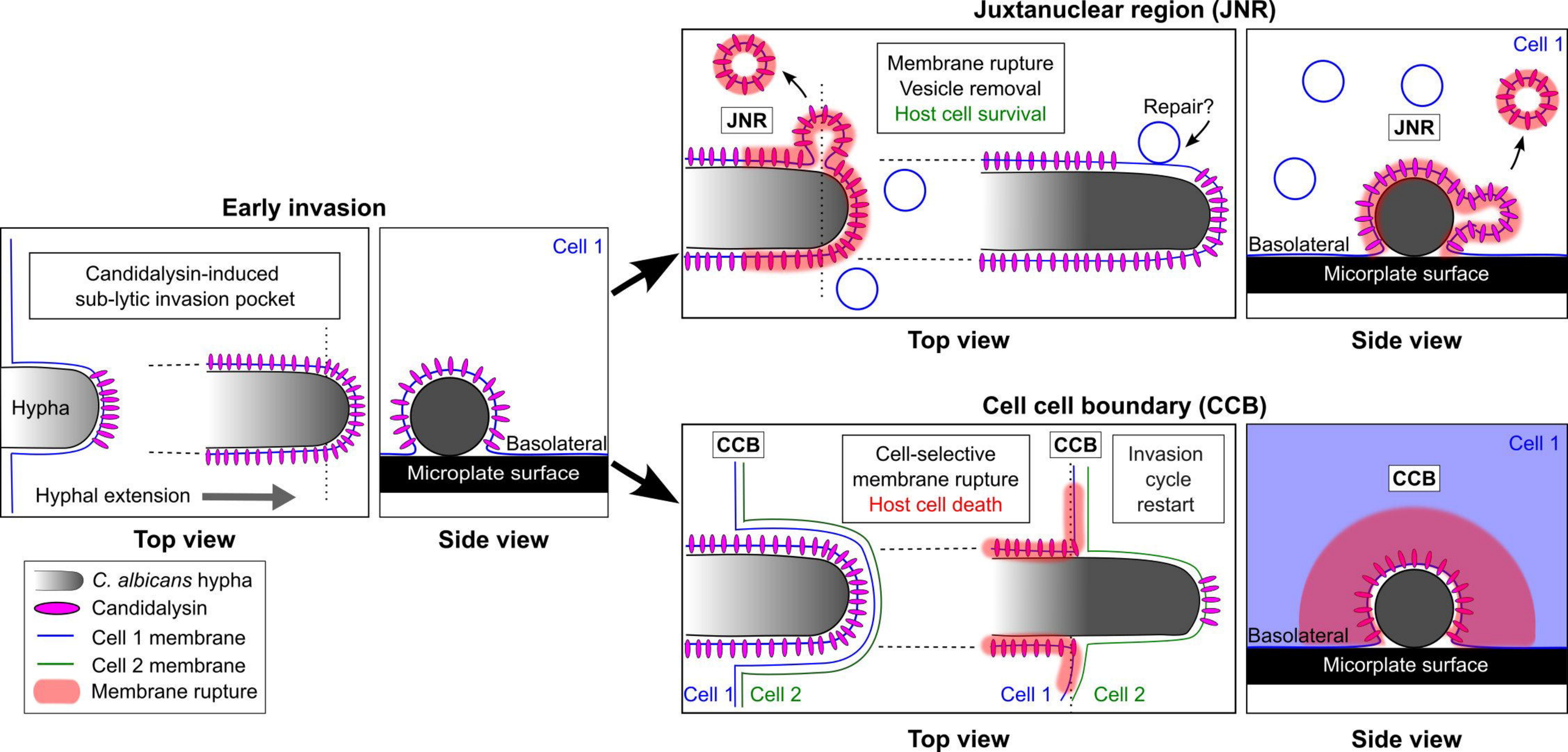
Juxtanuclear region (JNR)
Early invasion
Candidalysin-induced
sub-lytic invasion pocket
Hypha
Hyphal extension
Top view
Cell 1
Basolateral
Microplate surface
Side view
Membrane rupture
Vesicle removal
Host cell survival
JNR
Repair?
Top view
Cell 1
JNR
Basolateral
Micorplate surface
Side view
Cell cell boundary (CCB)
CCB
Cell-selective
membrane rupture
Host cell death
CCB
Invasion
cycle
restart
Cell 1
Cell 2
Cell 1
Cell 2
Top view
Cell 1
CCB
Basolateral
Micorplate surface
Side view
C. albicans hypha
Candidalysin
Cell 1 membrane
Cell 2 membrane
Membrane rupture